Università Campus Bio-Medico di Roma
School of Engineering

PhD Course in Biomedical Engineering
(XX - 2004/2007)

Novel Approaches to Functional Assessment and Interaction Control for Robot-aided Neurorehabilitation

Domenico Formica

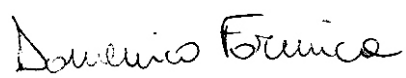

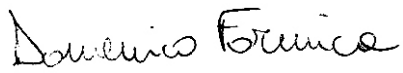

Novel Approaches to Functional Assessment and Interaction Control for Robot-aided Neurorehabilitation

A thesis presented by
Domenico Formica
in partial fulfillment of the requirements for the degree of
Doctor of Philosophy
in Biomedical Engineering

Università Campus Bio-Medico di Roma
School of Engineering

Coordinator
Prof. Saverio Cristina

Supervisor
Prof. Eugenio Guglielmelli

Co-Supervisors
Dr. Loredana Zollo
Prof. Paolo Maria Rossini

January 2008

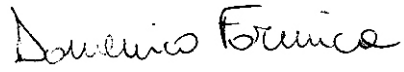

A papà, mamma, Giovanni e Giovanna, Vincenzo, Silvia

Domenico Formica

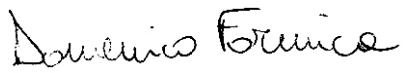

Abstract

It is commonly accepted that neuroplasticity is the basic mechanism underlying the recovery after brain injuries, and it has been widely shown that rehabilitation motor therapy can considerably influence recovery in patients with neurological diseases.

However, the neurorehabilitation is labor intensive, often given through a one-on-one patient-therapist relation, and relies on manual interactions with a trained therapist several hours a day. In addition, patient evaluation is often done subjectively, with the therapist making hands-on or visual judgments about a patient's movement abilities. This makes it difficult to monitor and evaluate treatment effects.

The introduction of appropriately designed machines could potentially enhance rehabilitation measurement by quantifying specific pathophysiological mechanisms, spontaneous recovery, functional ability, and therapy dosage more accurately than it is now possible. They could also help with therapy itself, replicating key components of current manual therapeutic techniques, or even applying new techniques, giving help in answering fundamental scientific questions and improving cost-efficiency of therapy.

The main objective of this work is to provide innovative solutions to improve functional assessment in hemiplegic patients and enhance the outcome of neurorehabilitation by customizing the motor therapy on the basis residual motor capabilities of each single subject.

To this purpose, this dissertation thesis presents, on the one hand, two algorithms to quantitatively analyze the clinical picture of patients with neuro-muscular disorders; on the other hand, it tries to provide innovative control solutions that could enhance the performances of the existing machines used in robot-mediated motor therapy and tailor therapy interventions to each patient's needs and abilities.

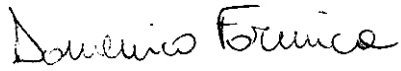

Contents

Domenico Formica

Domenico Formica

List of Tables

Domenico Formica

List of Figures

Domenico Formica

Domenico Formica

Domenico Formica

Domenico Formica

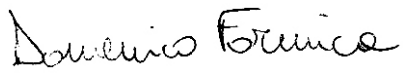

Chapter 1

INTRODUCTION

Nowadays brain injuries and consequent motor disabilities are a one of the most important and growing problem in healthcare. Stroke, for example, is the third cause of death behind heart disease and cancer and the leading neurological cause of long-term disability in the world. About 700000 people suffer a stroke each year only in the United States and in almost one half of the survivor, motor deficits persist chronically [1].

It is commonly accepted that neuroplasticity is the basic mechanism underlying the recovery after brain injuries, and it have been widely shown that motor cortex functions change depending on motor experiences; for this reason rehabilitation interventions can considerably influence post-stroke recovery and motor therapy is the main therapeutic treatment given to patients in sub-acute and chronic phase.

The rehabilitation after brain injuries is labor intensive, often given through a one-on-one patient-therapist relation, and relies on manual interactions with a trained therapist several hours a day. In addition, patient evaluation is often done subjectively, with the therapist making hands-on or visual judgments about a patient's movement abilities. This makes it difficult to monitor and evaluate treatment effects [2].

The introduction of appropriately designed machines might partially solve these problems and improve the efficacy of stroke recovery. Sophisticated devices that would attach to a patient's limb, measure movement and force generation, and apply therapeutic patterns of forces could make a significant impact on stroke rehabilitation management.

Such machines could potentially enhance rehabilitation measurement by

Domenico Formica

quantifying specific pathophysiological mechanisms, spontaneous recovery, functional ability, and therapy dosage more accurately than it is now possible. They could also help with therapy itself, replicating key components of current manual therapeutic techniques, or even applying new techniques, giving help in answering fundamental scientific questions and improving cost-efficiency of therapy.

The main objective of this work is to provide innovative solutions to improve functional assessment in hemiplegic patients and enhance the outcome of neurorehabilitation by customizing the motor therapy on the basis of residual motor capabilities of each single subject. More specifically the work presented here focuses mainly on the upper limb.

To this purpose, the present study presents, on the one hand, two algorithms to quantitatively analyze the clinical picture of patients with neuro-muscular disorders; on the other hand, it tries to provide innovative control solutions that could enhance the performances of the existing machines used in robot-aided motor therapy and tailor therapy interventions to each patient's needs and abilities.

In particular, at first two complementary works, aiming to improve the clinical assessment of neuro-muscular disorders of the upper limb, will be presented; then a bio-inspired interaction control for robot-aided motor therapy will be proposed and evaluated in comparison with the other traditional and bio-inspired controls proposed in literature.

This dissertation thesis is structured as follows:

- In Chapter 2 the neurophysiological assumptions of the use of motor therapy as a treatment for enhancing recovery of neurological patients are presented and discussed. A short review of the traditional techniques for neurorehabilittion commonly used in clinical practice are introduced. The state of the art of the existing robotic platforms for neurorehabilitation is revised and the main results of the validation of these technologies through clinical trials are underlined.

- In the following chapter two solutions are presented that aim to use novel technologies to clinically assess patients' level of disability through quantitative, reliable, reproducible techniques. The first one uses a commercial stereophotogrammetric system (VICON) for motion analysis to evaluate the level of impairment of the upper limb in hemilegic subjects. A biomechanical model have been developed and implemented to calculate several kinematic and dynamic variables starting from the VICON output varibles. The clinical experimentation involved four hemiplegic children, and

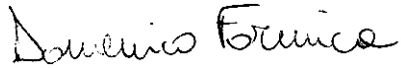

their performance were analyzed during pointing tasks executed at two different speeds. Several evaluation indexes have been introduced and their utility in discriminating natural from pathological behavior is evaluated by comparing results obtained from the healthy arm with those of the plegic one. The second work aims to develop a reproducible quantitative method to estimate the passive stiffness of the wrist joint using an existing wrist robot. In fact, abnormal muscle tone is one of the most important symptoms that affects patients with brain injuries and the evaluation of the passive mechanical properties of patients joints is often used as a basis for clinical assessment of neuro-muscular disorders. Nevertheless, clinical scales used to estimate the muscle tone are strongly operator-dependent and show high inter- and intra-subjective variability. In this work measures of wrist passive stiffness are carried out on 10 healthy subjects: a reproducible quantitative estimate of the wrist passive stiffness for flexion/extension, abduction/adduction and pronation/supination is separately calculated. Then the two-dimensional stiffness of the combined FE/AA movements is determined.

- In Chapter 4 a new control approach is proposed to manage interaction in robot-mediated motor therapy of the upper limb, that is purposively conceived for this application field. The control strategy tries to pave the way for developing control solutions able to answer the requirements of adaptability, safety, portability, and flexibility. The control law has been named *torque-dependent compliance control in the joint space* and its applicability to robot-aided motor therapy has been validated in comparison with another bioinspired interaction control previously presented in literature, the *coactivation-based compliance control law*.

Domenico Formica

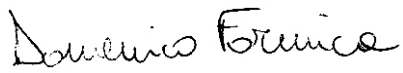

Chapter 2

NEUROREHABILITATION AND ROBOTICS: STATE OF THE ART

In this chapter the neurophysiological assumptions of the use of motor therapy as a treatment for enhancing recovery after brain injuries are presented and discussed. A short review of the traditional techniques for neurorehabilittion commonly used in clinical practice are introduced. The state of the art of the existing robotic platforms for neurorehabilitation is revised and the main results of the validation of these technologies through clinical trials are underlined.

2.1 Neurophysiological Rationale of the Role of Motor Therapy in Stroke Recovery

When a stroke occurs, a significant number of neurons and synaptic connection are suddenly lost by the cerebral tissue [3]. The magnitude of this infarct in such a focal area is problematic and reorganization of the remaining injured brain is very important for recovery to occur [4].

Even if the neurobiology of stroke recovery is poorly understood, it is commonly accepted that neuroplasticity is the basic mechanism underlying the recovery after brain injuries [5].

Understanding of the patterns of neurophysiological and physical recovery time post stroke can allow rehabilitation specialists to provide more effective therapy and improve use of resources during the patient's stay in hospital [6].

Domenico Formica

Partridge et al. have also suggested that an understanding of recovery and potential influencing factors can assist in the setting of an effective therapeutic strategies [7].

An example of factor that can influence recovery after stroke is the initial severity of the stroke; the "Copenhagen Stroke Study", conducted on 1197 stroke subjects, showed that the rate of neurological recovery is strictly related to the magnitude of stroke lesion [8]

Several studies showed that cerebral tissue close to the infarcted area exhibits a lot of structural modifications after stroke; in the same way, several neurons that are not adjacent to the lesion, but have structural connections with the affected part of the brain, participate in cortical reorganization [9, 10].

Research on monkeys and humans indicates that rehabilitation can enhance reorganization in the adjacent intact cortex and contribute to functional recovery after stroke [11, 12]. According to Teasell et al., Rehabilitation or training can increase cortical representation, whereas lack of rehabilitation decrease it [13].

One approach that has shown great promise in expediting progress toward stroke recovery in the upper extremity is activity-dependent motor rehabilitation interventions [14]. There is increasing evidence to suggest that in addition to injury-related reorganization, motor cortex functions change depending on motor experiences. Activity-dependent long-term modification of synaptic efficacy underlies information storage in neural networks. Thus, motor experiences, including rehabilitation interventions, considerably influence post-stroke recovery levels [15, 16].

Resuming, the neurophysiological assumptions for the use of motor therapy in the stroke recovery process can be described as follows:

1. Stroke recovery probably depends on neuroplasticity;

2. Motor activity strongly enhances neural plasticity process;

3. The stroke recovery process seems to exhibit the property of specificity, i.e. the benefits conferred to the not treated limbs are weak;

4. A common assumption is that stroke recovery is like motor learning, even though the role of abnormal tone, spasticity and other stroke sequelae is unclear.

Domenico Formica

2.2 Traditional techniques for neurorehabilitation

Comprehensive rehabilitation implies coordinated interdisciplinary care, comprising a broad spectrum of multidisciplinary interventions. Several neurological therapeutic approaches are advocated and applied, proponents of each one claiming its superiority in efficacy over the others. These approaches include:

- Bobath method [17].
- Neuro-developmental treatment (NDT) [18, 19].
- Brunnstrom method [20]
- Proprioceptive neuromuscular facilitation (PNF) [21, 22].
- Johnstone therapy [23].

Physical and occupational therapeutic programmes vary greatly from one facility to another as a result of the adherence to different treatment concepts [24, 25] and philosophies. For example, in the NDT method the emergence of basic synergies is considered as a pathological and undesirable manifestation of spasticity which should be suppressed in order to enable the facilitation of normal physiological movements. Contrary to this concept, Brunnstrom encourages the development of the same basic synergies and related spasticity in the pre-synergic phase of motor recovery. She claims this follows the natural sequence of motor recovery after stroke as first described by Twitchel [26]. To date the Bobath concept and its related or derived methods are believed to be the most popular and widely applied methods in stroke rehabilitation [27].

Within the last four decades a number of true-experimental and quasi-experimental group studies evaluating the efficacy of neurological therapeutic approaches have been published. These studies have been critically reviewed, but all reviewers shared the conclusion of Ernst that "it does not matter which approach is chosen and any of the available therapeutic approaches will improve the patients functional status" [28, 29, 30].

This conclusion is mainly based on the positive findings presented in the literature with respect to early initiated intensive rehabilitation in acute stroke patients.

2.3 Robot-aided Neurorehabilitation

The synergy between robotics and life science was born at the beginning of 80s, when several researches started using robotics technologies for neuroscientific

purposes. In those years many research groups tried to understand how the CNS plan and perform movements and many studies on human motion control have been carried out by measuring human motion properties through robotic platform [31, 32, 33].

At the beginning of 90s some of these robots, widely used in neuroscientific studies, have been modified and applied in the rehabilitation field, to assist the patients in motor recovery after cerebral injuries. Since then, the machines for assisted motor therapy have been considerably improved and applied to different fields, such as fitness, sports training, sensory-motor training for maintaining performance of elderly people and physical medicine and rehabilitation, with special attention to neurological pathologies (neurorehabilitation).

Machines currently used in most of the sports or rehabilitative training centers typically integrate a growing number of sensors, for proprioceptive perception, in particular for the measure of the trajectories of the mobile parts of the machine (and indirectly also of the patients limbs), as well as for exteroceptive perception, for the measure of the quantities that characterize the physical interaction with the human body (forces) and for monitoring the motor, cognitive and physiological parameters of the users. Such machines are therefore becoming mechatronic systems, with a central processing unit that can elaborate information recorded during motor exercises and, in the most advanced machines, with a system that can actively real-time control and customize the exercises depending on the subjective conditions of the single user and on the personal training strategy.

The evolution of these systems towards real robotic systems, with actuators that control the degrees of freedom of the machine based on the physical interaction with the user and, also, on the pre-programmed instructions and an adequate management of the sensors information during the exercise, may appear just an incremental evolution in terms of efficiency, functionalities and versatility oriented to the market in the field of robotic rehabilitation machines that is strongly growing. On the contrary, a more complex analysis of the potentialities of these systems [34] in view also of the recent neuro-scientific achievements (in particular as regards the mechanisms of neurogenesis and cerebral plasticity underlying the motor learning and the functional recovery after cerebral injury) highlights the advisability of using the robotic technologies to create a real discontinuity in the clinical procedures of the neurorehabilitative treatment.

Motor therapies where patients undergo passively the neurorehabilitators intervention, with poor participation of the high-level structures of the nervous system that are responsible for the imagination and the sensori-motor coordi-

nation and planning of the movements, may cause a low clinical efficacy of the functional recovery intervention with respect to the real possibility of improvement of the patients. To maximize patients functional recovery, research in the nerurorehabilitation field is oriented to therapies that favour motor exercises based on voluntary movements, often in a scenario of daily living activities. Moreover, the presence of severe neuromotor disabilities, that prevent patient from controlling basic motor activities such as the maintenance of erect posture, the deambulation and simple arm or hand movements, can highly limit the possibility of applying rehabilitative paradigms based on the active contribution of the patient by using the currently available technologies. From this point of view, it is clear that the availability of robotic machines for motor therapy could allow assisting also subject with low residual motor abilities, and help these patients start and complete motor tasks directly monitoring their motion intention, thus involving the cerebral structures that are at the basis of high level motion strategies, like in voluntary movements.

Many research groups have developed robotic devices for neuro-rehabilitation but only few of these have been validated by clinical experimentation [35]. The most widely tested in clinical practise are the following:

1. The InMotion systems (MIT-MANUS & Wrist robot) (see Fig. 2.1), developed by researches of the Massachusetts Institute of and commercialized by *Interactive Motion Technologies Inc.*, have been widely and successfully used in the last ten years in clinical trials that demonstrated how the robot-aided neurorehabilitation may complement other treatment approaches by reducing motor impairment in persons with moderate to severe chronic impairments [36, 37, 38]. The most recent studies show that they significantly improve motor abilities of the exercised limb segments in persons with chronic stroke [39, 40]. Nevertheless, the details of the recovery process remain largely unknown, so a deeper understanding is important to accelerate refinements of robotic therapy or suggest new approaches. For this purpose, robots provide an excellent instrument platform from which to study recovery at the behavioral level [41].

2. Mirror Image Motion Enabler (MIME) robotic device for upper-limb neurorehabilitation (see Fig. 2.2), developed and tested in the Palo Alto laboratories, have been used in studies where robot-aided therapy have been compared with conventional treatment [42, 43]. In these studies Robot-assisted treatment (bilateral, unilateral, and combined bilateral and unilateral) was compared with conventional therapy; authors claim that combined unilateral and bilateral robotic training have advantages

Domenico Formica

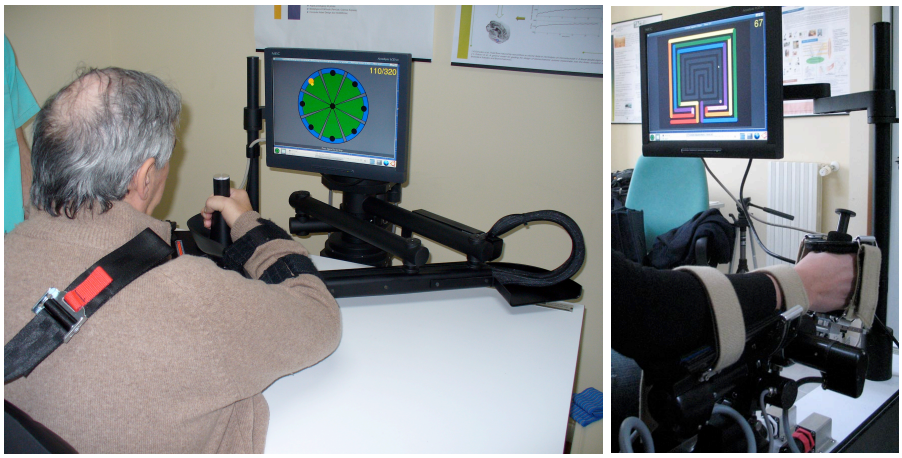

Figure 2.1: The InMotion$^{2\&3}$ systems (MIT-MANUS and Wrist robot) for robot-aided neurorehabilitation.

compared with conventional therapy, producing larger improvements on a motor impairment scale and a measure of abnormal synergies [44].

3. Assisted Rehabilitation and Measurement (ARM) Guide(see Fig. 2.3) measures and applies assistive or resistive forces to linear reaching movements across a wide workspace [45]. It consists of a hand piece that is attached to a linear track and actuated by a DC servomotor. The track can be oriented at different yaw and pitch angles to allow reaching to different workspace regions. It have been used to directly test the role of movement practice versus robotic forces in retraining reaching following chronic stroke [46].

4. The electromechanical gait trainer (GT I) (see Fig. 2.4) is based on a moving foot plate system [47], with cadence and step length that can be set individually. The first stroke studies with 30 acute stroke patients revealed improved gait ability and lower-limb muscle activity in chronic, nonambulatory stroke patients following 4 weeks of applied GT I training [48]. A recent multicenter trial, the DEutsche GAngtrainer-Studie (DEGAS), included 155 acute nonambulatory stroke patients [49]. The Experimental group scored significantly higher at the end of the study and at follow-up, on both Functional Ambulation Category (FAC) and

Domenico Formica

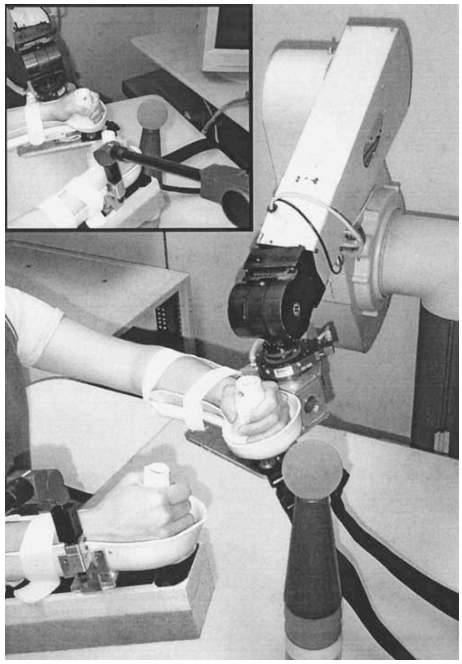

Figure 2.2: Mirror Image Motion Enabler (MIME) robotic device for upper-limb neurorehabilitation.

Barthel Index parameters, in respect of the control group. At the end of the study, 41 of 77 (53.2%) in experimental group versus 17 of 77 (22.1%) in control group could walk independently, i.e., they had reached an FAC level of either 4 or 5 [49].

5. The LOKOMAT system (see Fig. 2.5) is an automated gait trainer, developed by Hocoma (Switzerland) [50]. Since the Lokomat became commercially available in 2000, it has been used for gait training in individuals with various medical diagnoses. To date, several studies have examined the therapeutic and functional effects of gait training with the Lokomat in the SCI (Spinal Cord Injury), stroke, and TBI (Traumatic Brain Injury) patient populations [51, 52, 53, 54].

Several other robotic prototypes have been recently developed for robot-

Figure 2.3: The ARM guide rehabilitation system.

aided rehabilitation, but their application in clinical practice has not been deeply tested and validated. Some of them have been used in pilot studies that show the applicability of such devices to the rehabilitation context: the most promising examples are the Bi-Manu-Track [55], the MEMOS system [56], BRACCIO DI FERRO [57], the ARMin [58].

Domenico Formica

Figure 2.4: GT I electromechanical gait trainer. Harness-secured patient is positionedon two foot plates that when moved simulate stance and swing.

Figure 2.5: Lokomat robotic gait orthosis (Hocoma, AG , Volketswil, Switzerland).

Domenico Formica

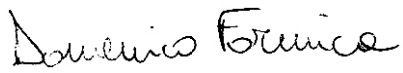

Chapter 3

METHODS AND TECHNIQUES FOR FUNCTIONAL ASSESSMENT OF THE UPPER LIMB

In this chapter two solutions are presented that aim to use novel technologies to clinically assess patients' level of disability through quantitative, reliable, reproducible techniques. First, a biomecanical model of the upper limb for the clinical assessment of motor impairment of hemiplegic children during pointing tasks is presented. Then, a reproducible quantitative method to estimate the passive stiffness of the wrist joint using an existing wrist robot is introduced and validated.

3.1 Evaluation of motor impairment of hemiplegic children during pointing tasks

3.1.1 Introduction

This section proposes a biomecanical model of the upper limb for the clinical assessment of motor impairment of hemiplegic children during pointing tasks. Accurate quantitative assessment of neuromotor deficits is essential in clinical application for choosing the appropriate treatment for the patients and monitoring recovery progress during rehabilitation. Established motor impairment

Domenico Formica

scales, such as the Fugl-Meyer, may be insensitive to small changes in impairment, have a very high subject variability, and are strongly operator-dependent.

Many previous approaches to analyze upper extremity motion did not allow a wide range of clinical applications [59]. Some were invasive [60, 61] or the setup restricted movement [62, 63, 61]. Other models simplify the upper extremity by neglecting some degree of freedom [61, 64, 65]. Several studies have examined reaching tasks in stroke subjects, but few incorporate upper extremity motion analysis [66]. The few existing upper extremity models lack validation, all degrees of freedom and 3D Euler joint angles [67, 65]. Data obtained from these models is often collected from a small sample population and with few cameras [68] or the evaluation of the impairment is carried out by only considering kinematic variables [59].

Despite the lack of application of biomechanical models to clinical practice, several studies have used systems of motion analysis to model the execution of upper limb movements of heathy subjects.

Since the early 1950s, several investigators have modeled the upper limb using various discrete masses, linear springs, and viscous dampers [69]. Previous mathematical analysis included the following assumptions: bones and tissues were considered rigid bodies, with their center of gravity fixed at a point, and joints were considered frictionless [70, 71, 72].

Optical systems with high resolution in space and time have been used to record 3-D kinematics of the upper limb [73]. A sensing garment that detects upper limb postures and movements has also been developed [74]. Analyses of upper limb movements are generally performed by measuring kinematic variables of the links and joints with accelerometers, electrogoniometers, or cameras [75, 76].

Several experimental approaches have been developed to measure joint moments. Joint moments can be measured by torque transducers during isometric tasks or by torque motors during dynamics tasks [73, 77]. All of these experimental approaches for measuring kinematics, forces, and moments restrict natural movement, require certain calibration and extra mounting fixtures, and can be invasive. Consequently, 3-D biomechanical models of the whole [70] or partial [78, 60, 79, 80] upper limb have been developed.

These models have used optimization methods to compute muscle forces and limb postures. Nieminen et al. used a 3-D model to predict maximum shoulder strength [80]. Raikova used mathematical analysis and the Denavit-Hartenberg (D-H) method to calculate position, muscle forces, and joint reactions for the upper limb [70]. Khalili and Zomlefer developed an approach to estimate the body segment parameters in a 2-D system for rehabilitation robotics [81]. In-

verse dynamics can be used to calculate the upper limb reaction forces and moments at a joint. Kinematics represent the movement of the link-segment model, while inverse dynamics derive the kinetics responsible for that movement. Recently, Abdullah et al. [82] have developed a dynamic biomechanical model for assessing and monitoring robot-assisted upper-limb therapy.

Moreover, in the last twenty years, several neurophysiological models have been proposed to understand and explain the way the brain plans and executes skilled movements in healthy subjects.

The analysis of kinematic and dynamic features of limb movements provides useful information about the control processes governing arm movements. The study of invariant characteristics of human movements under different conditions (speeds, amplitudes or direction of movements and different externally applied forces) led to different theories on how the central nervous system chooses from an infinite number of possible motor plans and solves biological redundancy. In fact, even if any motor task can theoretically be achieved by an infinite number of possible trajectories, human movement patterns are highly stereotyped; many studies have shown that subjects tend to move their hand along a straight path with a single-peaked, bell-shaped velocity profile [83]. This consistency is characteristic of a computational approach known as optimal control, in which a "cost" is specified as a function of the movement, and the motor output with the lowest cost selected [84].

Early studies of trajectory formation considered cost functions such as minimum energy, minimum torque, and minimum acceleration [85]. Hasan [86] has suggested that the cost function is the integrated "effort" of movement, where effort is defined as the product of muscle stiffness and the square of the derivative of the equilibrium point position.

At present only two cost functions are able to account for the majority of the multijoint data: the cost functions based on the Cartesian "jerk" (Minimun Jerk Model) [87, 31] and on the first derivative of torque (Minimum Torque-Change Model) [33].

The main purpose of this study is to use a 3D biomechanical model of the upper limb for a quantitative estimation of motor impairment in hemiplegic children during pointing tasks. A sophisticated system for motion analysis (VICON system) has been used to record kinematic variables of children's upper limb during pointing movements and a 3D model has been developed to calculate kinematic as well as dynamic variables. These variables act as input for the calculation of several evaluation indexes of motor impairment, and an analysis of motor performances of each subject have been carried out for both plegic and unimpaired arm. Using the unimpaired arm as a benchmark of the

motor performance the single subject can perform, a quantitative evaluation of the level of disability has been measured and proposed as an assessment of neuromotor deficits of such patients.

3.1.2 Materials and Methods

Subjects

Four hemiplegic children (two male and two female), having an average age of MEAN ± SD, have been involved in this study; they have been recruited among the patients of the Paediatric Neuro-Rehabilitation Division of the Children's Hospital "Bambino Gesù". The main characteristics of the subjects involved in the experimentation are listed in Table 3.1.

Table 3.1: Overview of the main characteristics of the hemiplegic children involved in the study.

	Age	Weight [Kg]	Height [cm]	Affected arm	Gender
Subject A	10	36.5	144	Right	Male
Subject B	8	22.5	115	Left	Male
Subject C	9	23.6	120	Left	Female
Subject D	11	41	149	Right	Female

Experimental Setup

The kinematics of the movement was analysed by means of a six-camera motion capture system (Vicon 512, Oxford Metrics, UK). The sampling rates were set at 120 images per second. Static and dynamic calibration tests, performed in accordance with the manufacturer's indications, showed that overall RMS error of marker coordinates in three-dimensional space was less than 1 mm.

VICON system automatically calculated the position of centers of rotation of shoulder, elbow and wrist which have been used as input of the biomechanical model. Trials were also videotaped to provide a permanent record and to assist in clinical interpretation of data.

During the experiments, EMG signals of the five main muscles of the shoulder have been recorded to verify the muscular activation patterns in the execution of the motor tasks.

Figure 3.1 shows an example of the experimental setup during an evaluation session with the VICON system.

Domenico Formica

Figure 3.1: The experimental environment and setup during an evaluation session with the VICON system.

Experimental protocol

Subjects were placed in the large experimental room and asked to stand in resting position. Experimenters instructed the subjects to point their index finger to the wall in front of them and to go back to the resting position, without stopping between upward and the downward movement.

Subjects executed the task at two different speeds, normally-paced speed and fast speed, with both unimpaired and plegic arm; instructions to the subjects were "make the movement using your comfortable speed", for the normally-paced speed, and "move as fast as you can" for the fast speed.

The experimental protocol consists of nine movements for each level of speed with both the arms, for overall thirty-six movements for each subject. No instructions were given about the hand's path and arm posture. Movement

Domenico Formica

accuracy was not the primary constraint on subjects during these experiments.

Data analysis

The coordinates of the centers of rotation (COR) of shoulder, elbow and wrist joints provided by the VICON system were used as input to the data analysis. Positions of CORs were low-pass filtered and numerically differentiated to obtain velocities and accelerations.

After visual inspections of each single trial, movement onset was defined as the instant which linear tangential velocity of the wrist COR exceeded 5 % of its peak; on the other hand, the end of movement was defined as the instant when the same velocity dropped below the 5 % threshold, as done in a previous work by Papaxanthis et al. [88]. Each pointing movement have been divided into two different components: upward component, that is the part of the movement performed against gravity, and downward component; the time used to separate the two parts of the movement has been defined as the time at which the vertical component of the wrist velocity changes its sign.

Kinematic and dynamic models of the upper limb have been developed to obtain from the COR positions further kinematic (such as angles, velocities and accelerations of human joints), dynamic (such as torques applied by the muscles) and energetic (such as potential and kinetic energy and powers related to each joint) variables.

The model consists of four 1-degree of freedom (i.e. DOF) revolute joints and two rigid bodies (links). The revolute joints model the DOFs of the shoulder joint (in the following sequence: internal/external rotation, abduction/adduction and flexion/extension) and the elbow flexion/extension. The two links connect the shoulder COR to the elbow COR and the elbow COR to the wrist COR, representing the upper arm and forearm respectively.

Figure 3.2 shows the kinematic diagram of the proposed biomechanical model and the sequence in which the different DOFs are defined. The model represents the shoulder as a 3-DOF spherical joint (the glenohumeral joint) and the elbow as a 1-DOF joint (elbow flexion/extension). The wrist joint was not included in the model because its movements were considered irrelevant for the specific task. For this reason, the wrist COR was considered the end-effector of the model. Moreover, the following assumptions were made for this application: bones and tissues were considered rigid bodies, with their center of gravity fixed at a point, and joints were considered frictionless.

The lengths of upper arm and forearm were calculated as the distances between two subsequent CORs, and mass, moment of inertia and center of

Domenico Formica

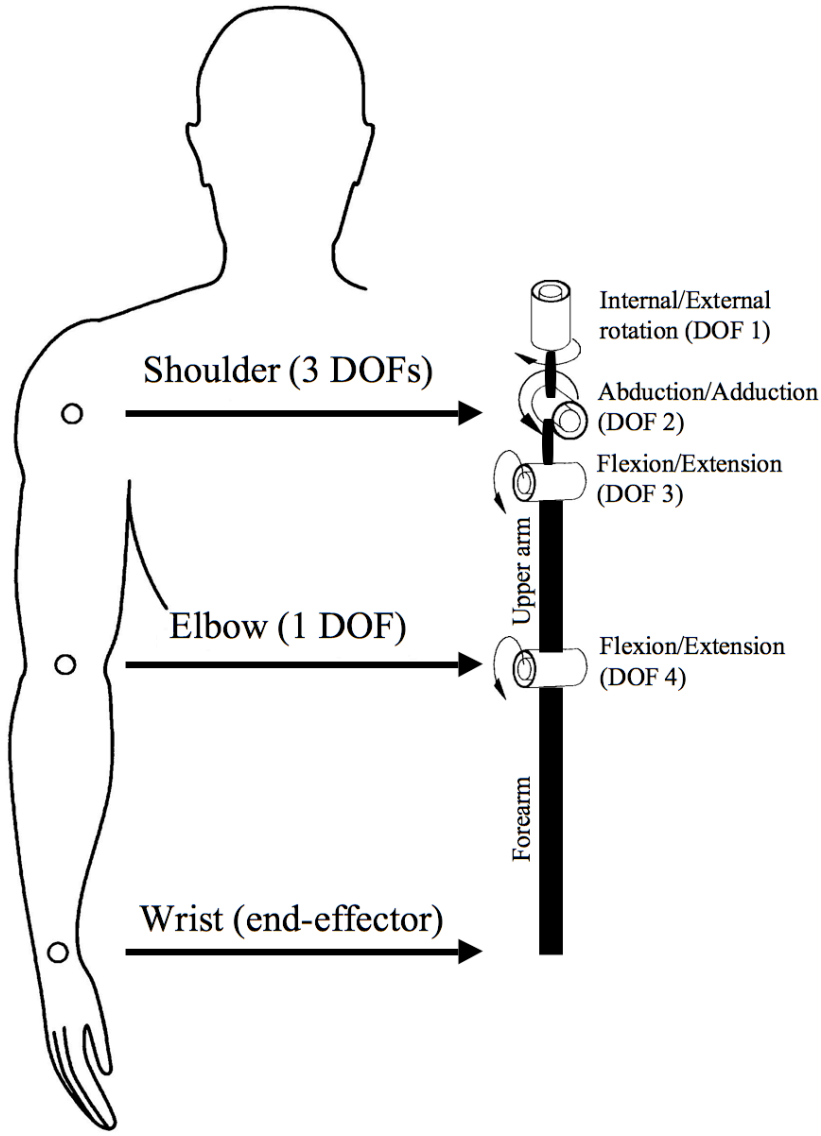

Figure 3.2: The kinematic diagram of the proposed biomechanical model and the sequence in which the different DOFs are defined.

Domenico Formica

mass for the upper arm and forearm were estimated for each subject using the average anthropometric parameters given in literature [77].

EMG signals of shoulder muscles have been used to verify the presence or absence of voluntary muscles contraction during the different phases of the movement. The developed 3D biomechanical model uses as input the shoulder, elbow and wrist centers of rotation and can be used to calculate the following sets of variables:

- Kinematic variables: angular positions, velocities and accelerations of each DOF of the model;
- Dynamic variables: Inertial, Coriolis and Gravitational components of joint torques for each DOF of the model;
- Energetic variables: potential and kinetic energy of the system, powers related to each DOF of the model;
- EMG activation patterns for each variable.

The kinematic and dynamic model has been implemented with the SimMechanics toolbox of MATLAB (The MathWorks Inc., USA); Fig. 3.3 shows a snapshot of the graphical interface of the proposed model.

Using the original and calculated variables, several indexes have been estimated to evaluate motor performance of subjects, and quantitatively assess the motor impairment of the plegic arm. Most of them have been suggested by the previous studies on human motor planning and execution of movements in healthy subjects [87, 33, 88]. The evaluation indexes uses in this study can be resumed as follows:

1. **Kinematic Indexes**. They are based only on kinematic variables and are calculated as described below:
   - *Movement Duration* (MD): it is the time the subject takes to perform the movements. The duration of the movements is calculated between the onset time and the ending time as previously described. MDs for Upwards and downwards movements are calculated separately.
   - *Peak Velocity* (PV): it is the maximum values of the velocity magnitude of the wrist COR during upwards and downwards movements.

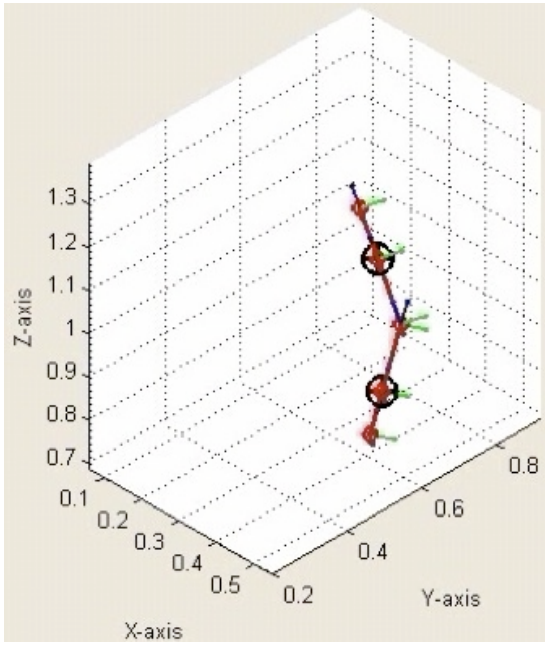

Figure 3.3: A snapshot of the graphical interface of the proposed model, implemented in SIMMECHANICS/MATLAB environment.

- *Time to Peak Velocity* (TPV): it is the percentage time (with respect to the Movement Duration) the subject spends to reach the Peak Velocity. This index characterizes the movement timing because gives information on the relation between acceleration and deceleration time of one single movement. For planar point-to-point reaching movements, it has been shown that this parameter is equal to 0.5 (same acceleration and deceleration time) [31], but it can be modified by changes in the physical constraints, such as movements against gravity [89, 90].

- *Peak to Mean velocity Ratio* (PMR): it is the ratio between the peak and the mean velocity magnitude of the wrist COR. This index describes the shape of velocity profiles: for planar movements at minimum jerk (which maximize the smoothness of the movements),

Domenico Formica

it is equal to 1.875 [31], but it assumes different values during movements against gravity, depending on the direction of the movement (upward or downward) [88].

- *Jerk Index* (JI): it is calculated by dividing the mean jerk (derivative of the acceleration) magnitude by the peak speed. This index has been suggested by Rohrer et al. [91] as a measure of movement smoothness in post-stroke patients; in fact, the jerk metric characterizes the average rate of change of acceleration in a movement; hence an increase of the JI corresponds to a decrease of smoothness.

2. **Cost Indexes**. They are based on cost functions used in neurophysiological studies to model and understand the way the brain plans and executes point-to-point movements. Since these indexes have been proposed as the cost functions that brain tries to minimize when executes healthy movements, they could be very useful in detecting pathological behaviors of plegic movements when compared to healthy ones. In this study only the cost functions related to the two main motor control theories have been taken into account:

   - *Jerk Cost Function* (C_J): it was originally proposed by Hogan [87] for one-joint and Flash and Hogan [31] for multijoint movements, and states that the cost function the brain tries to minimize is the first derivative of Cartesian hand acceleration (i.e. jerk). Thus, the C_J is calculated as follows:

$$C_J = \frac{1}{2}\int_0^T \left(\left(\frac{d^3x}{dt^3}\right)^2 + \left(\frac{d^3y}{dt^3}\right)^2 + \left(\frac{d^3z}{dt^3}\right)^2 \right) dt \qquad (3.1)$$

     where T is the duration of the movement and x, y, z are the coordinates of the wrist COR at time t. To compare the values of this index in movements performed at different speeds, the jerk function in (3.1) has been normalized in magnitude (dividing by the maximum value of jerk magnitude) and in time.

   - *Torque-change Cost Function* (C_T): it was proposed by Uno et al. [33] as an alternative approach to trajectory planning and generation. The minimum torque change model differs from the minimum jerk model in that the reference trajectories are dependent on the dynamics of the arm. In this study, C_T has been evaluated as fol-

Domenico Formica

lows:

$$C_T = \frac{1}{2}\int_0^T \left(\left(\frac{d\tau_1}{dt}\right)^2 + \left(\frac{d\tau_2}{dt}\right)^2 + \left(\frac{d\tau_3}{dt}\right)^2 + \left(\frac{d\tau_4}{dt}\right)^2\right) dt \quad (3.2)$$

where T is the duration of the movement and $\tau_1, \tau_2, \tau_3, \tau_4$ are the torques calculated by the model for the four different DOFs. As for C_J, torques in (3.2) have been normalized in magnitude and time.

Statistical analysis

For each subject the average values and the Standard Error (SE) for all the indexes detailed above were calculated. Significant differences on all the indexes between healthy and plegic arm were tested using a two-tailed t-test and the statistical significance was accepted when $P < 0.05$.

3.1.3 Results

Figure 3.4 shows the typical profile of wrist velocity magnitude of slow movements, performed with both healthy and plegic arm; in all the figures, the parts of the movements where EMG activity is present are drawn in green. Velocity plots clearly show that healthy movements are smoother than plegic ones. Healthy paths have a single velocity peak in both upward and downward movements. On the contrary, plegic movements exhibit secondary peaks besides the main one and in downward movements velocity amplitude drops quickly after the first peak. In particular, this last aspect seems to be strictly correlated with the absence of EMG activity in the second part of downward plegic movements, differently to what happens in healthy movements.

For fast movements (see Fig. 3.5), the differences between healthy and plegic arm are not evident: obviously pathological movements are always slower (as demonstrated by Movement Duration and Peak Velocity values presented in the next section), but the shape of velocity profiles is quite similar for the two conditions. As regard EMG signals, activation patterns show very clear and reproducible differences between healthy and plegic movements, in both slow and fast conditions. The main characteristics can be resumed as follows:

- In slow movements with the healthy arm, EMG is always active during all the movement in both upward and downward directions;

Domenico Formica

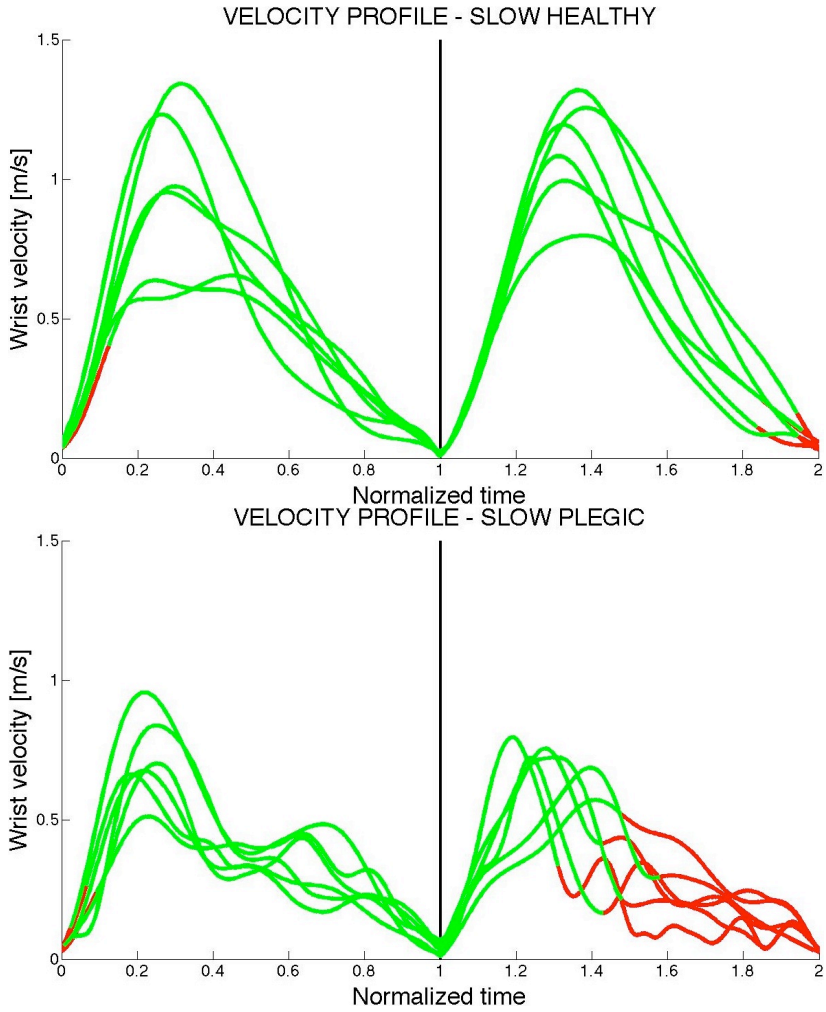

Figure 3.4: Wrist velocity magnitude of slow movements performed with healthy (top) and plegic (down) arm. The normalized time goes from 0 to 1 for upward movements and from 1 to 2 for downward movements. The parts of the movements where EMG activity is present are drawn in green.

Domenico Formica

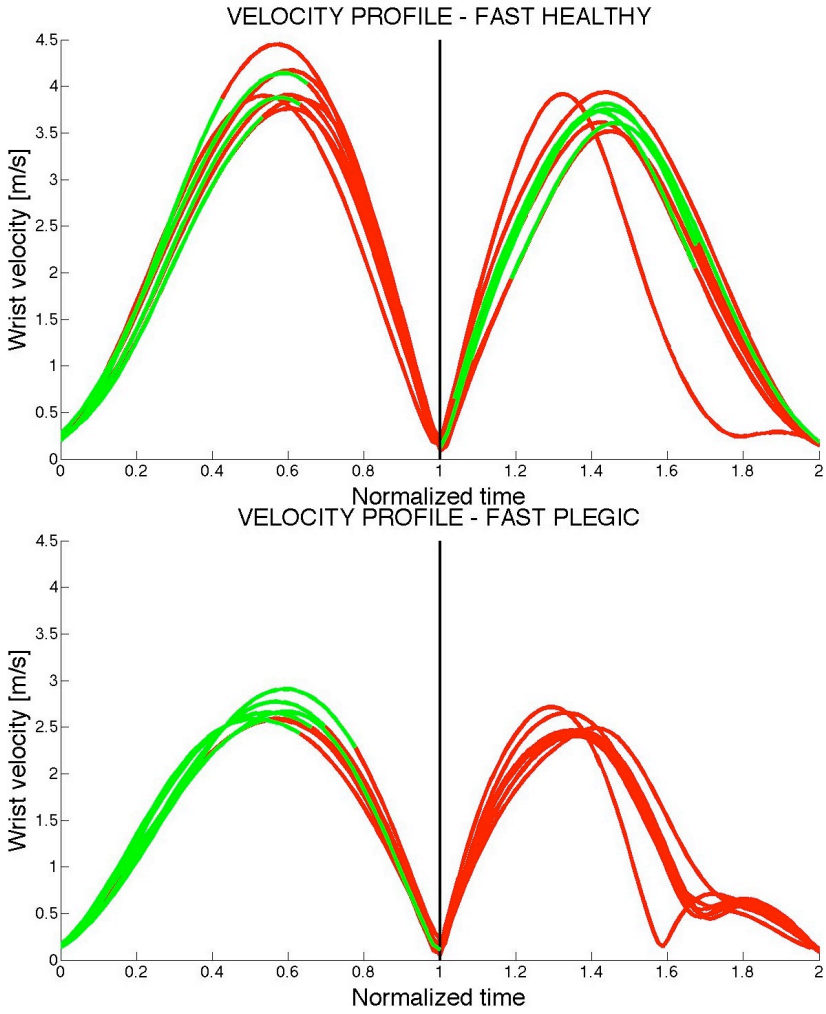

Figure 3.5: Wrist velocity magnitude of fast movements performed with healthy (top) and plegic (down) arm. The normalized time goes from 0 to 1 for upward movements and from 1 to 2 for downward movements. The parts of the movements where EMG activity is present are drawn in green.

Domenico Formica

- In slow movements with the plegic arm, EMG is active during all the upward movement but it disappears in the second half of the downward movement;
- In fast movements with the healthy arm, EMG is active from the onset of the movement until the wrist reaches the maximum speed and becomes silent during the last part of the upward movement; EMG activity reappears in the first part of the downward movement;
- In fast movements with the plegic arm, EMG is active only in the first half of the upward movement; it is always silent in downward movements.

This stereotyped behavior of EMG signals can be usefully related to the total power exerted by shoulder muscles during the movements; it has been calculated by summing the power associated to the three different shoulder DOFs of the model. In Fig. 3.6 power plots of slow movements performed by one representative subject are shown. In healthy movements the power course appears to be quite symmetric, with a negative peak during the downward movements similar in shape and amplitude to the positive peak exhibited in the upward movements. On the contrary, in trials with plegic arm power goes rapidly to zero and assumes values very close to zero during all the second half of downward movement, when EMG is silent.

More interesting remarks can be done for fast movements: power plots show definite differences between healthy and plegic movements corresponding to the distinct characteristics in EMG signal. In particular, during the first half of downward movements where EMG is present in the healthy arm and absent in the plegic one, power exhibits a relatively long period with positive values (about 40 % of the downward movement) that is not present at all in plegic movements. This behavior suggests that subjects actively control the healthy arm in upward as well as downward movements; on the other hand they do not actively control the plegic arm in downward movements.

Movement Duration and Peak Velocity

Figure 3.8 shows the average duration of fast and slow movements for both arms and movement directions. As it can be noted, values of MD for slow movements are very similar for all the 4 conditions and no statistical differences have been found between healthy and plegic arm.

For fast movements, MD values are obviously smaller for healthy arm in both upward (healthy: 0.39 ± 0.011 s (SE); plegic: 0.45 ± 0.015 s) and downward

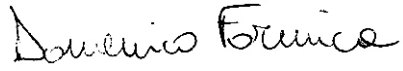

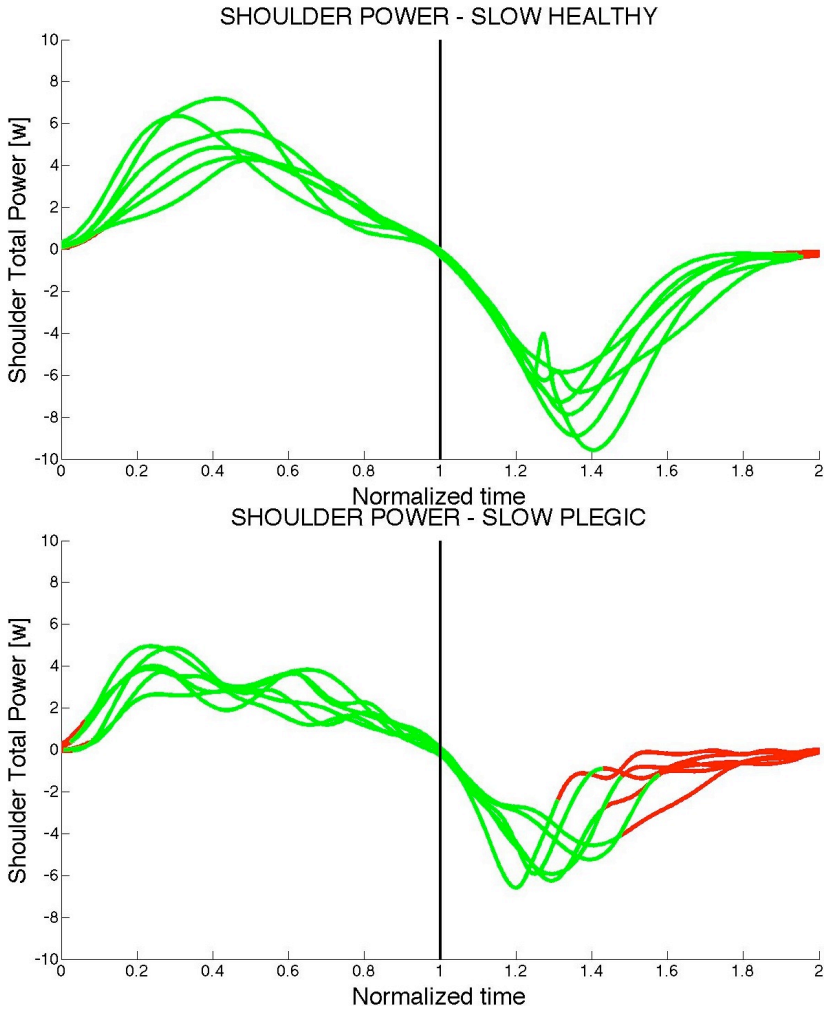

Figure 3.6: Shoulder total power of slow movements performed with healthy (top) and plegic (down) arm. The normalized time goes from 0 to 1 for upward movements and from 1 to 2 for downward movements. The parts of the movements where EMG activity is present are drawn in green.

Domenico Formica

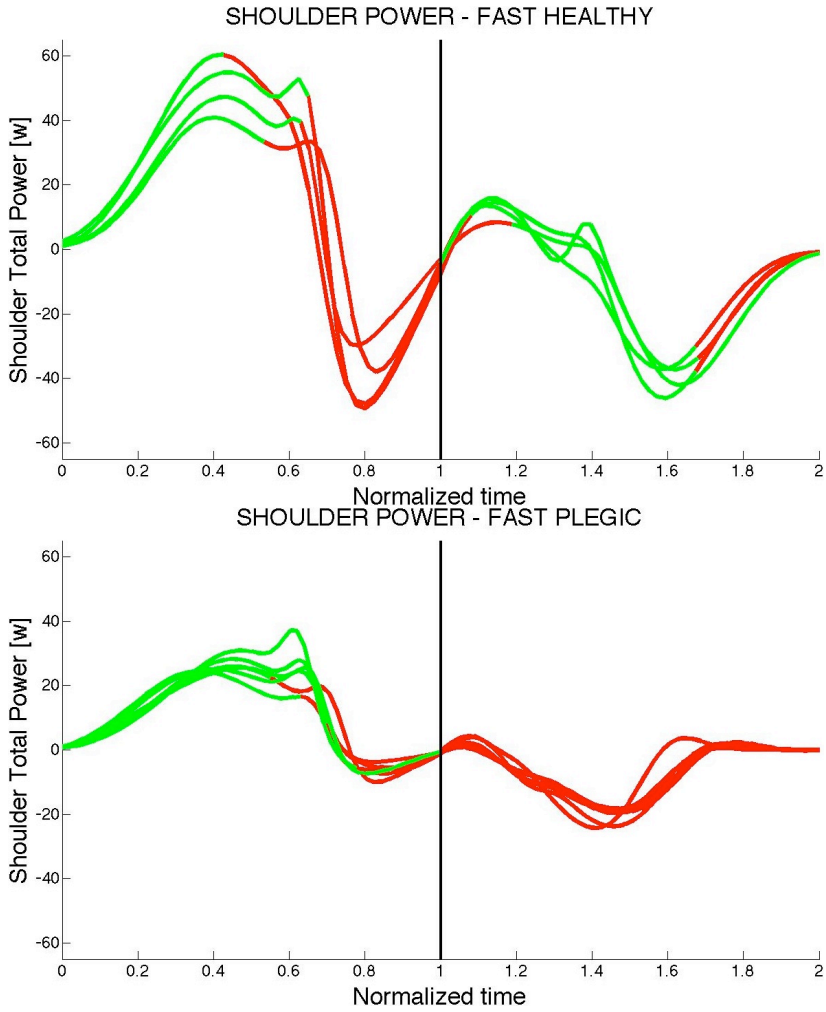

Figure 3.7: Shoulder total power of fast movements performed with healthy (top) and plegic (down) arm. The normalized time goes from 0 to 1 for upward movements and from 1 to 2 for downward movements. The parts of the movements where EMG activity is present are drawn in green.

Domenico Formica

(healthy: 0.50 ± 0.016 s; plegic: 0.62 ± 0.020 s) directions. It is worth noting that for both the arms downward movements takes always longer than upward ones. All the differences are statistically significant ($P < 0.05$).

Duration of movements has of course a strict correlation with peak velocity values, shown in Fig. 3.8. As previously stated for MD index, statistically significant differences have been found between healthy and plegic fast movements for both upward (healthy: 3.78 ± 0.124 m/s; plegic: 3.32 ± 0.104 m/s) and downward (healthy: 3.40 ± 0.079 m/s; plegic: 2.95 ± 0.064 m/s) directions.

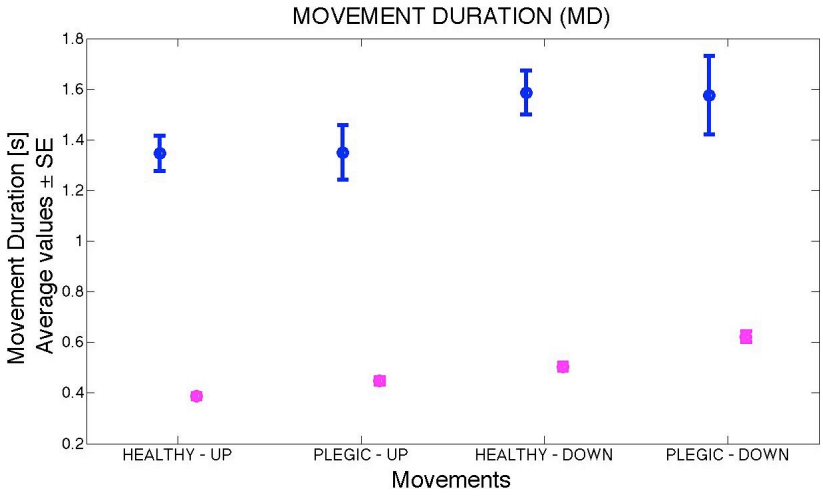

Figure 3.8: Average values and standard errors of MD index for slow (blue) and fast (pink) movements.

Time to Peak Velocity and Peak to Mean velocity Ratio

As shown in Figs. 3.4 and 3.5, velocity profiles exhibit different behavior in the various testing conditions. These characteristics can be usefully analyzed by using shape, as quantified by the ratio of Peak to Mean velocity Ratio (i.e. the PMR index), and the timing, quantified by the ratio of acceleration time to overall movement duration (i.e. the TPV parameter).

As regards the TPV during slow trials, it does not show significant changes in the four conditions (see Fig. 3.10), except for the downward movements

Domenico Formica

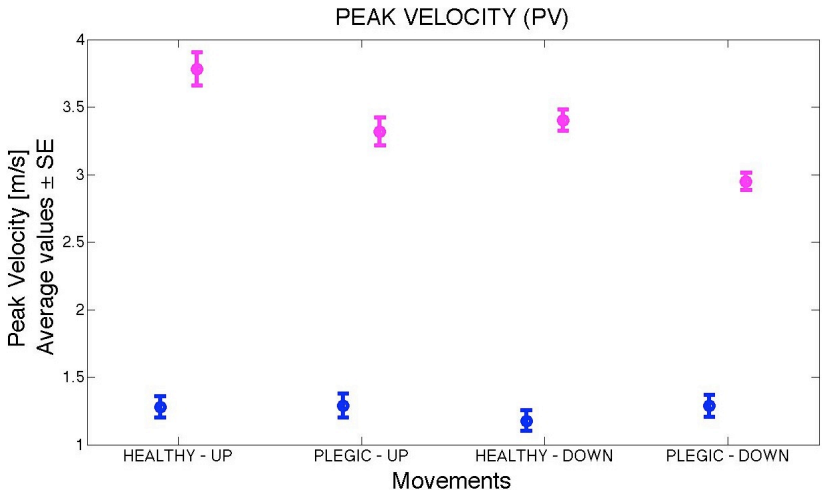

Figure 3.9: Average values and standard errors of PV index for slow (blue) and fast (pink) movements.

with the affected arm where it assumes higher values (0.47 ± 0.027). In fast experiments, TPV is strongly different in upward movements with respect to downward ones, but it does not show any significant difference between healthy and plegic limb (healthy UP: 0.57 ± 0.013; healthy DOWN: 0.37 ± 0.015; plegic UP: 0.57 ± 0.015; plegic DOWN: 0.37 ± 0.014).

Concerning the timing of movements, the PMR index does not show any significant difference in slow movements for the different conditions. In fast tests, as already stated for TPV parameter, the PMR index varies between upward and downward movements but it is not useful to quantify differences between pathological and healthy behavior (see 3.11).

Jerk metric

Jerk metric has been successfully introduced by Rohrer et al. [91] as a measure of movement smoothness in post stroke patients. As expected, in slow movements healthy arm exhibit a smoother behavior (i.e. JI lower) with respect to the plegic one (see 3.12). JI values are considerably lower (differences highly significant) in healthy movements than in plegic ones, in both upward (healthy: 15.5 ± 1.11 $1/s^2$; plegic: 20.4 ± 1.40 $1/s^2$) and downward (healthy: 13.5 ± 0.76 s;

Domenico Formica

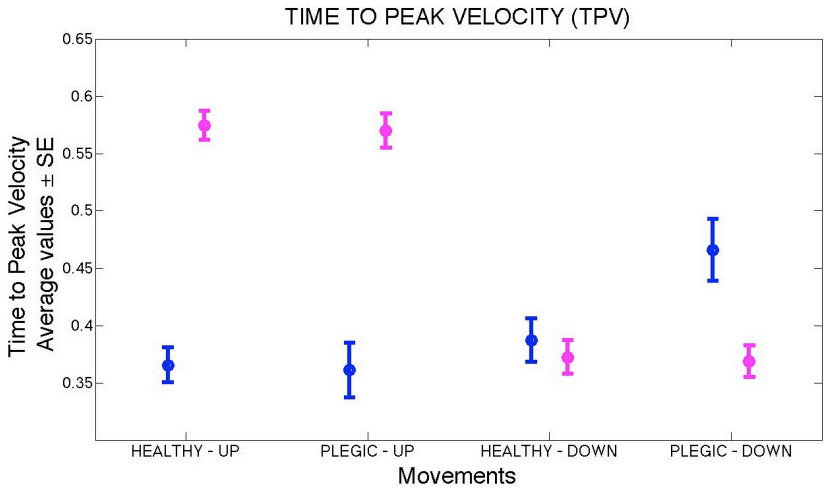

Figure 3.10: Average values and standard errors of TPV index for slow (blue) and fast (pink) movements.

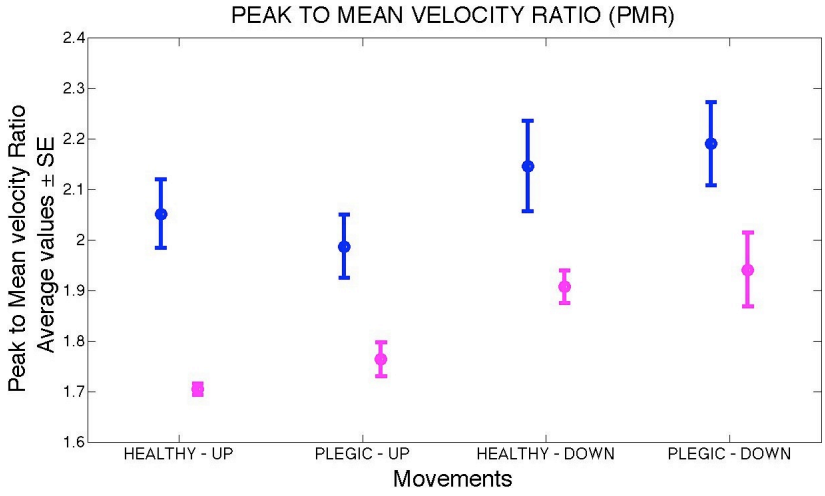

Figure 3.11: Average values and standard errors of PMR index for slow (blue) and fast (pink) movements.

Domenico Formica

plegic: 19.7 ± 1.54 $1/s^2$) directions. On the contrary, during fast movements JI values are extremely higher for healthy movements in both motion directions (healthy UP: 113.6 ± 8.71 $1/s^2$; healthy DOWN: 83.9 ± 4.77 $1/s^2$; plegic UP: 88.5 ± 5.07 $1/s^2$; plegic DOWN: 68.6 ± 4.82 $1/s^2$), contrary to what it can be supposed (see discussion). In Fig. 3.12 Jerk Index values are represented.

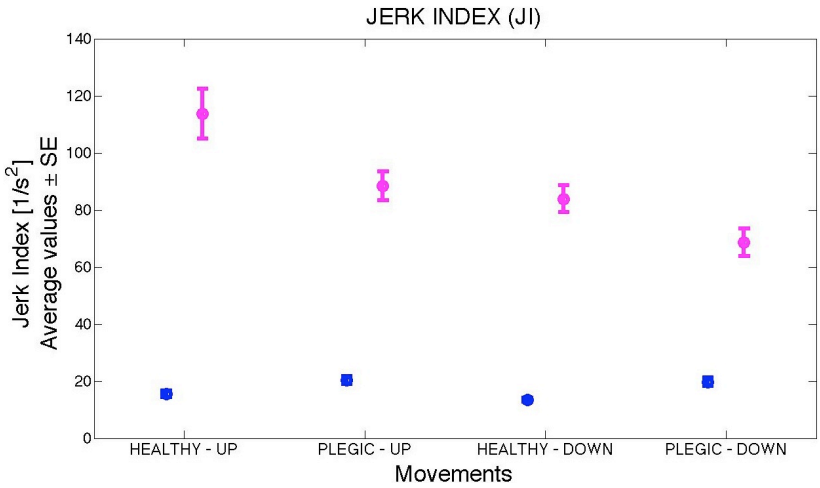

Figure 3.12: Average values and standard errors of Jerk Index (JI) for slow (blue) and fast (pink) movements.

Cost indexes

Jerk Cost Function (C_J) and Torque-change Cost Function (C_T) have been widely used in neurophysiological models of human movements as functions optimized by the brain when performs point-to-point tasks. For this reason they have been used in this work as indexes capable of distinguishing between pathological and healthy movements.

Figure 3.13 represents values of C_J and shows that no differences between healthy and plegic arm have been found in upward movements for both slow and fast trials. On the other hand, C_J values are higher for plegic arm with respect to the healthy one in downward movements (healthy slow: 0.115 ± 0.010; plegic slow: 0.131 ± 0.012; healthy fast: 0.173 ± 0.008; plegic fast: 0.207 ± 0.010), even if this difference is statistically significant only for fast trails.

Domenico Formica

Concerning the C_T (see Fig. 3.14), its values in slow tests are statistically different in both downward and upward movements, with plegic values higher than healthy ones (healthy UP: 0.147 ± 0.018; plegic UP: 0.191 ± 0.016; healthy DOWN: 0.099 ± 0.015; plegic DOWN: 0.156 ± 0.019). In fast movements a statistically significant difference has been found only in downward movements (healthy: 0.129 ± 0.013; plegic: 0.156 ± 0.011); this confirms that in fast movements the most relevant differences between healthy and plegic behavior can be found mainly in downward movements, as demonstrated by the differences in EMG activation patterns and in power plots (see 3.7).

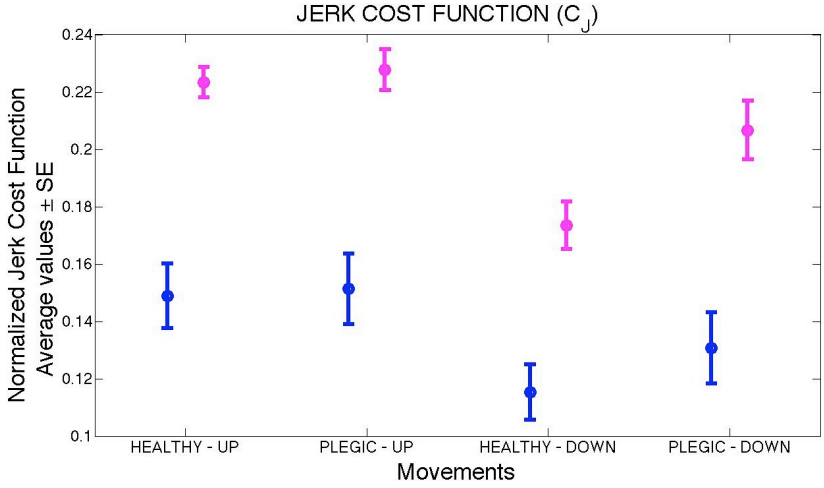

Figure 3.13: Average values and standard errors of Jerk Cost Function (C_J) index for slow (blue) and fast (pink) movements.

3.1.4 Discussion

The main goal of this study is to find some reproducible quantitative indexes capable to assess motor impairment in hemiplegic children. A very simple motor task (pointing movements a two different speed, normally-paced and fast) have been chosen to this propose and several parameters have been evaluated.

A global eloctrophysiological evaluation have been made by monitoring the EMG of the main shoulder muscles during the experiments. Strong and consistent activation patterns seem to distinguish healthy from plegic behavior,

Domenico Formica

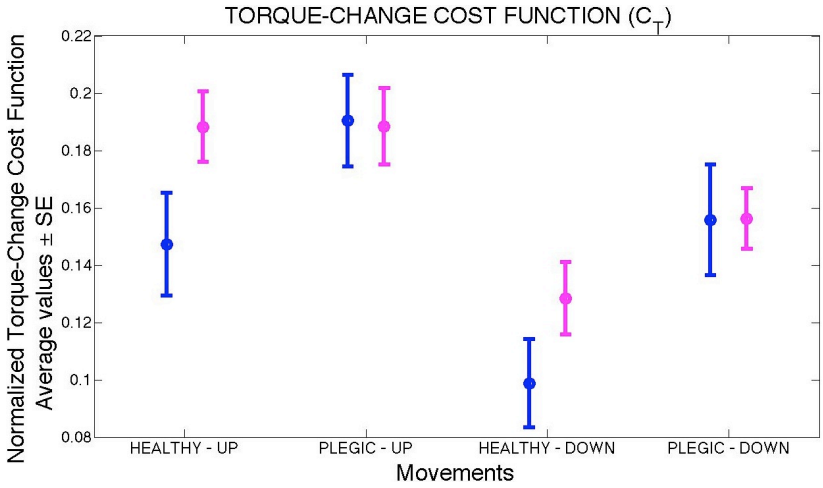

Figure 3.14: Average values and standard errors of Torque-change Cost Function (C_T) index for slow (blue) and fast (pink) movements.

expecially in downward movements. In particular, it clearly results that during fast trails subjects actively drive the healthy arm in the downward part of motion but not the plegic one.

It have been shown that Movement duration and consequently Peak Velocity don't highlight any significant difference when children are asked to move at their comfortable speed. At slow speed, subjects chose to move their limbs at the same average velocity, even if perform movements with the plegic limb. On the other hand, when fast movements are required, healthy arms can move faster then plegic ones; so, Movement Duration and Peak Velocity indexes strongly change between tasks with healthy or plegic limb.

Results indicate that global characteristics of velocity profiles such as shape (PMR index) and timing (TPV index) are not able to account for differences between healthy and plegic limb; for this reason, they can not be used in this context as evaluation indexes.

On the other hand, the use of the Jerk Index (JI), purposively thought to quantify movement smoothness and successfully used in previous studies [91], can strongly discriminate between healthy and plegic behavior of slow movements. As qualitatively shown in Fig. 3.4, plegic movements are considerably less smooth than healthy ones, and this results in a difference of 25%-30% in the

Domenico Formica

Jerk Index. As regards fast movements, it is clear that movement smoothness is not the main concern, because plegic movements appear to be as smooth as healthy ones (see 3.5). Moreover it seems that JI is strongly affected by movement speed as demonstrated by the enormous difference in JI values between slow and fast trials(see 3.12). For this reason, it can be supposed that JI values of healthy arm assumes higher values with respect to the plegic arm, due to the difference of about 15% in average velocity.

This lack of resolution of JI can be overcome by using the Jerk Cost Function. Values of JCF show a different statistically significant in downward fast movements, where plegic arm exhibits higher values of JCF index. Similar results have been found using the Torque-change Cost Function, that underlines difference between plegic and healthy behavior in slow movements (both upward and downward) as well as in the downward part of the fast movements. This common difference of cost indexes in downward fast movements demonstrate that the brain is not able to optimize Jerk Cost Function and Torque-change Cost Functinon in the same way when controls healthy or plegic limb. This result also explains the differences showed by EMG signals when fast movements are performed in downward direction.

3.2 Wrist Passive Stiffness Estimation

3.2.1 Introduction

Abnormal muscle tone is one of the most important symptoms that affects patients with brain injuries. For this reason, the evaluation of the passive mechanical properties of patients joints is often used as a basis for clinical assessment of neuro-muscular disorders. Several clinical scales are used to estimate the abnormal muscle tone. The most popular of these scales are the Modified Ashworth Scale (MAS) [92], the Tardieu [93], and the Pendulum tests [94]. Widespread use of a scale does not imply high reliability [95, 96, 97]. A more quantitative measurement of the mechanical characteristic of tone could be valuable for both assessment of stroke patients as well as understanding of posture and human movement. Here we focus on the development of a reproducible quantitative method to estimate the passive stiffness of the wrist joint using an existing wrist robot [98]. The measurements provided in this study are related to the wrist passive stiffness of each DOF separately (FE, AA and PS) and to the combined 2D stiffness of the FE and AA DOFs. While healthy subjects were recruited for this study, the proposed method is general and is presently being tested in post-stroke clinical studies. Over the past years,

Domenico Formica

several studies have focused on the mechanical properties of the human arm during both maintenance of posture or movements [99, 32, 100, 101, 102, 103]. These studies showed that the shoulder-elbow muscles have a predominant spring-like behavior [32] and that the measured stiffness ellipses vary depending on the arm configuration and during movements [102]. Furthermore, it has been shown that the CNS regulates the end-point arm stiffness to stabilize unstable dynamics [104]. While there is significant understanding of the shoulder and elbow stiffness, little is known about the wrist joint. There were attempts to estimate the total dynamic impedance during co-contraction [105] and quantify reflex contribution separately [106]. Lakie et al. [107] estimated the wrist flexion-extension passive stiffness by measuring the resonance frequency of the FE DOF; Leger and Milner [108] analyzed the response of the wrist joint during FE movements applied by a manipulator and Axelson and Hadberth [109] investigated the wrist stiffness in extended position. All these studies focused only on a single degree of freedom of the wrist joint (flexion-extension). To our knowledge, there were no studies of wrist passive stiffness in abduction-adduction (AA) and pronation-supination (PS). In this study, we first moved each degree of freedom of the wrist separately at a constant velocity. We measured the torque and displacement during movement determining a reproducible quantitative estimate of the wrist passive stiffness for FE, AA, and PS. We then determined the two-dimensional (2D) passive stiffness of the wrist joint in the FE/AA plane. We employed the same analytical techniques used in the past by others to determine the characteristic of the arm including the determination of the distribution of conservative and non-conservative components of stiffness [32].

3.2.2 Materials and Methods

Subjects

Ten right-handed healthy subjects were involved in this study (7 males and 3 females; mean age 30.1 y.o., range 24 to 42) with no history of neuromuscular disorders. Subjects volunteered to participate in the study in accordance to requirements of MIT COUHES (Committee on the Use of Humans as Experimental Subjects).

Experimental Setup

We employed a novel wrist robot capable of moving simultaneously in FE, AA and PS degrees of freedom (for details see [98]). We selected an impedance

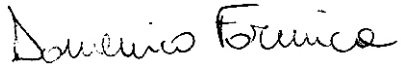

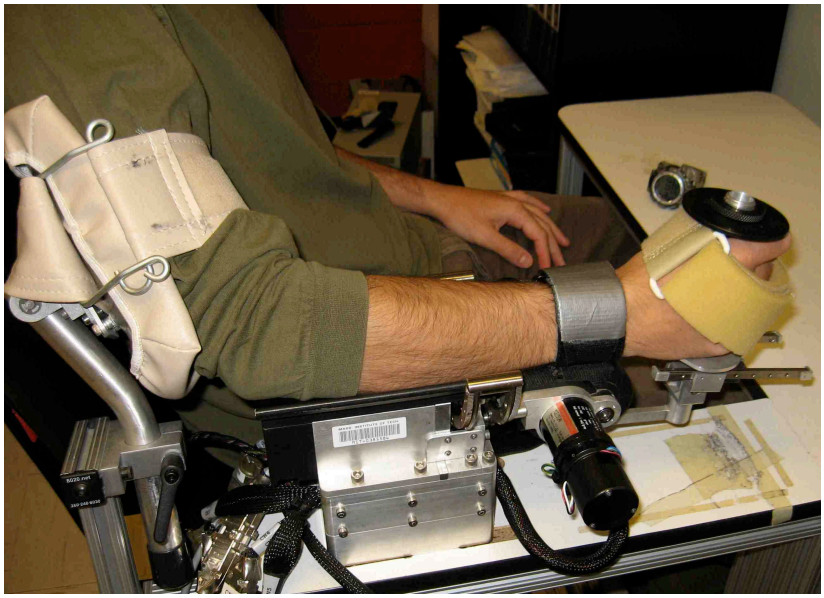

Figure 3.15: Set-Up: The forearm is fixed in 130 extension, with FE, AA and PS unrestrained only in the desired movement direction. Axes of rotation are aligned with the torque motors. The handle is designed to allow radial deviations.

controller with position and velocity feedback gains of K = 10 Nm / rad and B = 0.1 Nm s / rad respectively. The wrist robot records joint displacements, velocities, and torques of which we used the recorded joint angles and commanded torques to estimate stiffness. All the stiffness estimates were corrected for the hardware inherent bias; the hardware bias was estimated by adding a weight to the handle similar to the average human hand (approx. 0.30 Kg). The apparent stiffness bias occurs because of the changing moment arms with respect to the center of mass. Subjects were seated in a chair with their right shoulder in scaption position, while their forearm was fixed horizontally at 130 elbow extension (see fig. 3.15). The wrist joint was unrestrained only in the tested DOF.

Domenico Formica

Protocol

We instructed subjects not to interfere with the movement. Two different kinds of approaches were used in this study: the 1-D protocol, designed to measure the passive stiffness of FE, AA, PS in isolation and the 2-D protocol, used to calculate the combined stiffness of the wrist in the FE/AA plane. The 1-D protocol consisted of constant-speed movements with the constant-speed and the range of movement as variables. The goal was to verify that our stiffness estimation was insensitive to different movement parameters. Each condition was repeated 4 times and we observed no statistical differences among the different trials with different speeds and range of movement. Figure 3.16 shows a representative example of position and velocity profiles of the robot imparted movement. To neglect joint viscosity and to avoid evoking reflexes, robot velocity was kept very low in all the trials (less than 0.2 rad/sec). The 2-D bi-dimensional protocol consisted of robot movements along 24 equally-spaced directions in the FE/AA plane, as it is shown in fig. 3.17. Robot movement does not pause between two consecutive movements.

Data Analysis

The recorded variables used in the data analysis were the angles and the commanded motor torques of the three DOF of the wrist robot (FE, AA, PS).

For the 1-D protocol, we estimated passive wrist stiffness of the linear parts of the angle-torque curves. We excluded the non-linearity caused by the apparent hysteresis.

We analyzed the data collected during the 2-D protocol in two different ways:

1. The first approach, called the fitting ellipse method, consisted of splitting the data in 48 different constant velocity movements and aligning both torques and angles at the origin. We then obtained the components of torques and angles parallel and orthogonal to each movement direction. To estimate stiffness for each direction, we run a linear regression between torques and angles parallel to each direction and estimated the mean value per direction. The mean values for each of the 24 movements (outbound and inbound) were used to fit a stiffness ellipse. This approach major advantage is that it permits to estimate the distribution of the stiffness in the FE/AA plane without any particular a-priori assumptions about symmetry. It allows for the estimated stiffness in one direction to be different from the opposite direction (with respect to the

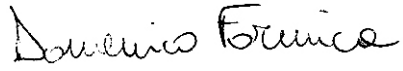

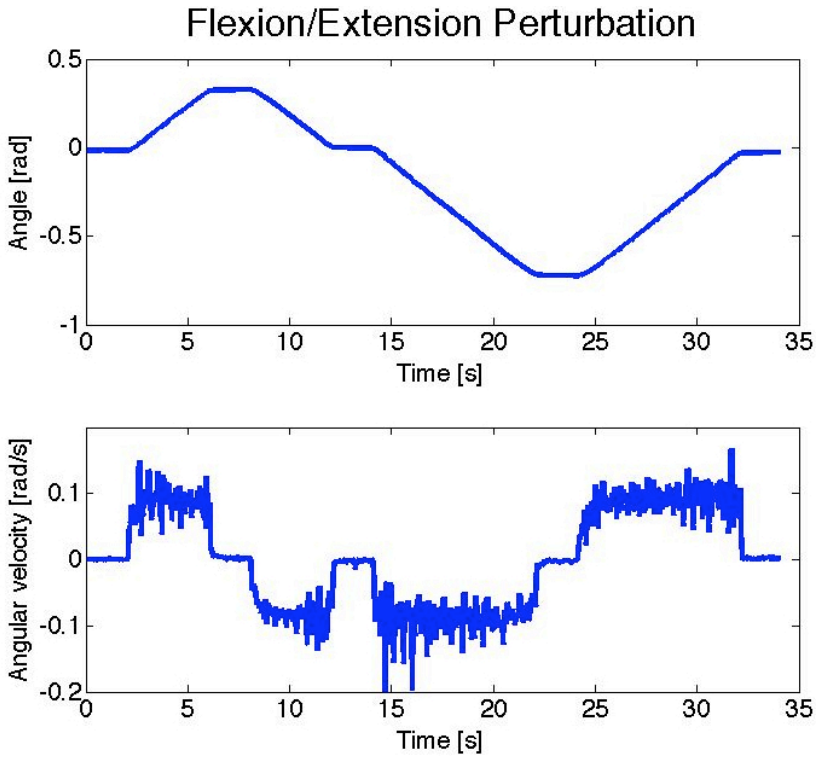

Figure 3.16: Position and velocity profiles of one perturbation of the FE DOF. This was applied all the three DOFs at different velocities.

origin of the reference frame). On the other hand, this approach major handicap is that it does not take into account orthogonal components and hence, cannot be used to analyze the relationship between the conservative and non-conservative components of the stiffness.

2. To overcome this limitation, we developed a 2nd approach to account for the orthogonal component and compare the conservative with the non-conservative characteristics of stiffness tensor. It employs a multivariable linear regression method in which we separate the outbound from the inbound movements, while shifting both torques and angles to the origin. We then estimated three stiffness tensors for the inbound

Domenico Formica

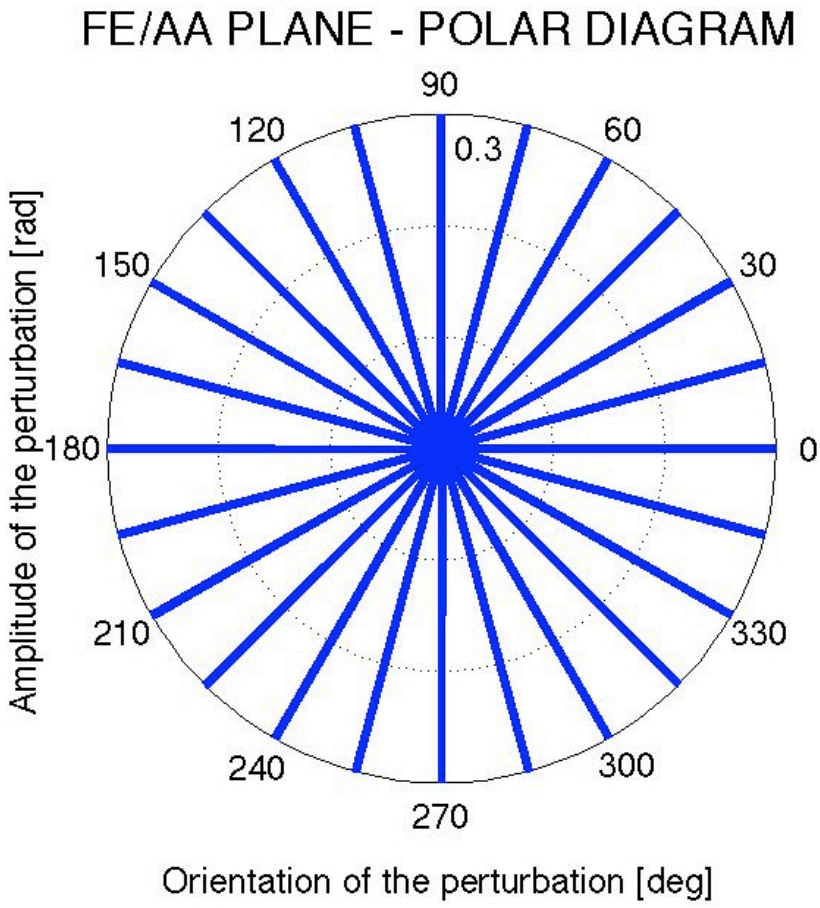

Figure 3.17: Orientation and amplitude of the 24 movements in the FE/AA plane used in the 2-D protocol.

Domenico Formica

movements, for the outbound movements, and for the composite of both. Such an approach permits the separation of the stiffness tensors into symmetric and antisymmetric matrices and affords the comparison between the non-conservative and conservative components of the stiffness. We adopted Mussa-Ivaldis graphical representation for the symmetric and anti-symmetric components [32].

3.2.3 Results

1-D Protocol

Figures 3.18, 3.19 and 3.20 depict typical plots of the angle-torque curve for the different DOFs. Note that the angle-torque curve has a linear behavior, and therefore the wrist passive stiffness can be estimated using a linear regression. The slope of the curve is not symmetric with respect of the two sides of the neutral position and all curves resemble a hysteresis loop. For all the three DOFs, the linear parts of the angle-torque curves give the estimation of 4 stiffness values, two for each side of the neutral position. For the FE and AA DOFs, the linear stiffness estimates were highly correlated, with an R^2 coefficient of 0.958 $\pm$ 0.029 (mean $\pm$ SD) for the FE and 0.928 $\pm$ 0.063 for the AA. Lower values of the R^2 coefficient were observed for the PS (0.605 $\pm$ 0.104), probably due to the gear design. Figures 3.21, 3.22 and 3.23 and Table 3.2 shows the wrist stiffness estimates for the 10 unimpaired subjects. For each DOF, the stiffness values were corrected for the hardware apparent bias stiffness. Of notice, the stiffness estimates on both sides of the neutral position were statistically significant different for the FE and AA degrees of freedom, the stiffness values related to the two different sides of the neutral position are highly statistically different (α=0.05, FE and AA: $p<0.01$). The differences between the pronation and supination stiffness are not significant.

2-D Protocol

Figure 3.24 shows a typical example of the results obtained by using the fitting ellipse method. The polar representation of the wrist FE/AA stiffness shows the values of the stiffness along the different directions and the fitted ellipse. Note that for all subjects, the data has quite smooth shape which is well approximated by an ellipse. The stiffness ellipse is not centered in the origin of the reference frame, which confirms the results coming from the 1-D protocols

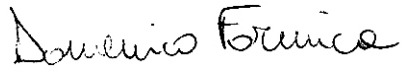

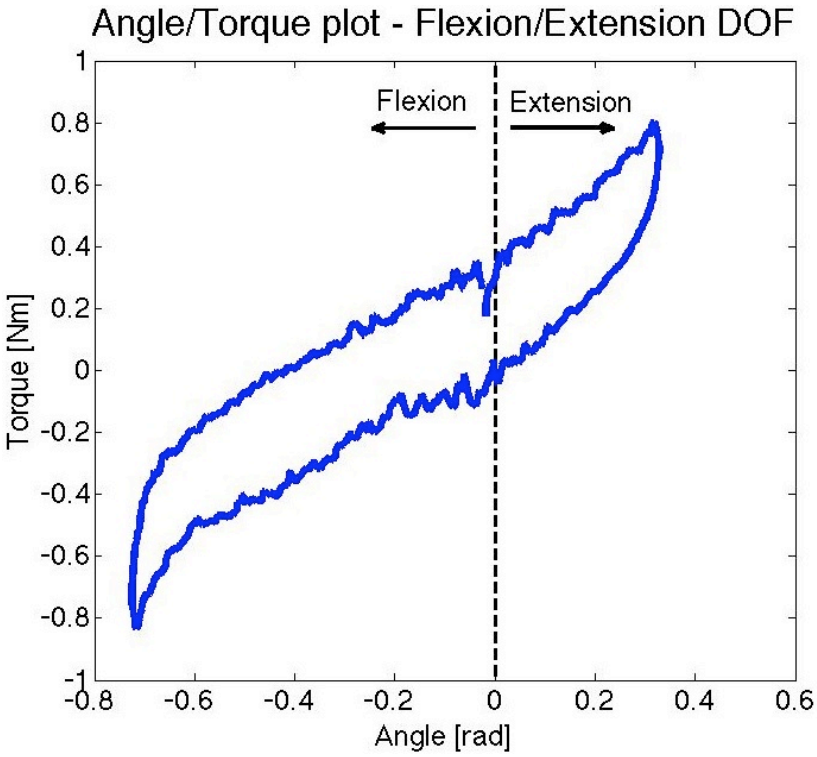

Figure 3.18: A typical torque/angle curves for one representative subject for flexion/extension.

(i.e.: extension stiffness higher than flexion and abduction higher than adduction). Furthermore, the two axes of the stiffness ellipse are not aligned with the axis of the reference frame, but the ellipse is counterclockwise tilted for right handed subjects. The linear regressions between torques and angles parallels to each direction showed very high correlation. The mean R^2 value, averaged over the 48 linear regressions for each subject and over all the 10 subjects, was 0.948 ± 0.025 (mean $\pm$ SD). The estimated stiffness ellipse approximates quite well the stiffness values: the mean R^2 value, averaged over the 10 subjects, was 0.880 ± 0.061. Table 2 shows the results for the 10 enrolled subjects. Note that the fitting ellipse method allows for asymmetry of the elastic field with respect

Domenico Formica

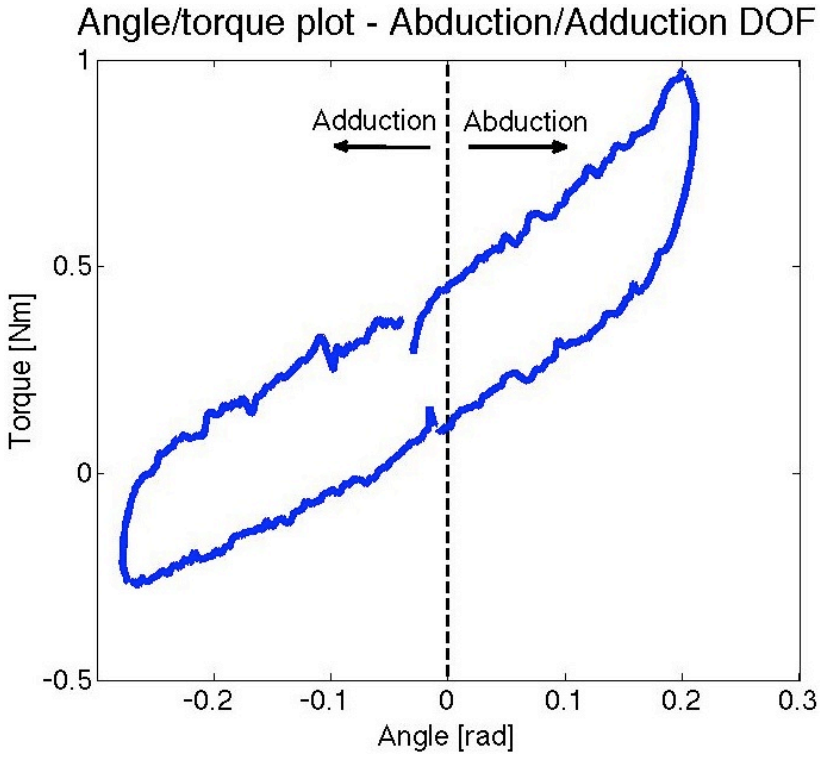

Figure 3.19: A typical torque/angle curves for one representative subject for abduction/adduction.

of the neutral position. To evaluate the relation between the conservative and non-conservative components of the elastic force field, we used the multivariable linear regression between the torque vector (FE and AA torques) and the angle vector (FE and AA angles) and estimated three stiffness tensors as described earlier. The regressions showed very high correlation values. The R^2 value average was 0.947 ± 0.031 for the inbound movements; 0.935 ± 0.023 for the outbound; and 0.924 ± 0.025 for the composite. Figure 3.25 shows an example of the stiffness ellipses obtained via this method; in drawing the ellipses only the symmetric component of the stiffness tensors has been considered, as suggested by Mussa-Ivaldi (REF). Table 3.3 shows the comparison of the two

Domenico Formica

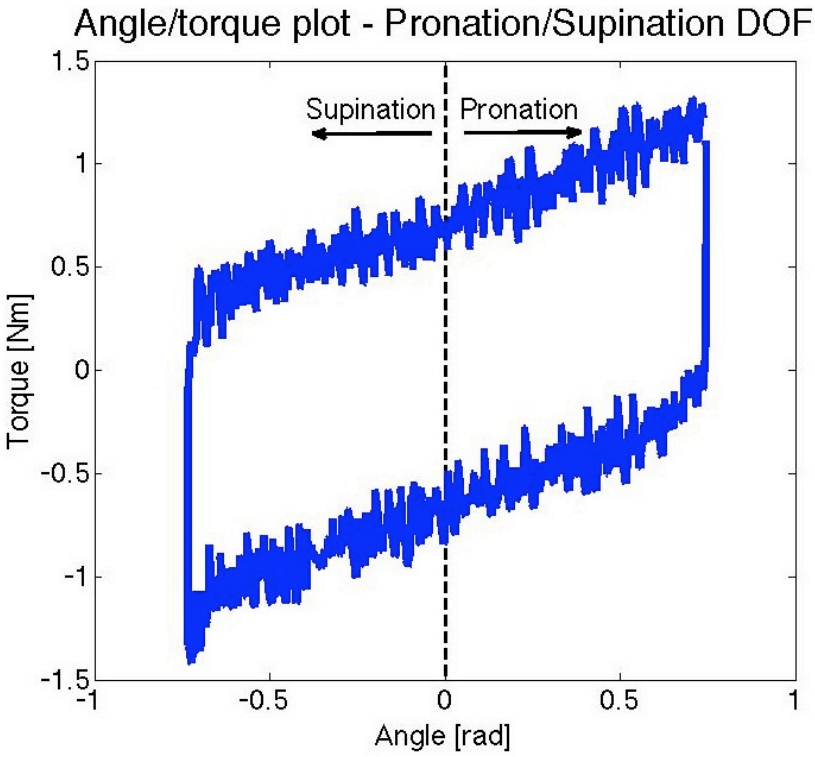

Figure 3.20: A typical torque/angle curves for one representative subject for pronation/supination.

methods: the fitting ellipse method and the multivariable linear regression.

Note that the magnitude of the stiffness ellipses (represented by the ellipse area) appears to be quite dependent on the estimation method. However, the eccentricity is very similar across different estimation methods. The orientation of the ellipse appears to be insensitive to the estimation methods for the same subject, even if it showed a quite high intra-subject variability . Nevertheless, for all subjects, the stiffness ellipses are tilted in the same way. Finally, the curl values were used to quantify the non-conservative component of the elastic field. The ratio between the determinant of the anti-symmetric part of the stiffness and the determinant of the symmetric part is near zero (0.003 ± 0.004; see

Domenico Formica

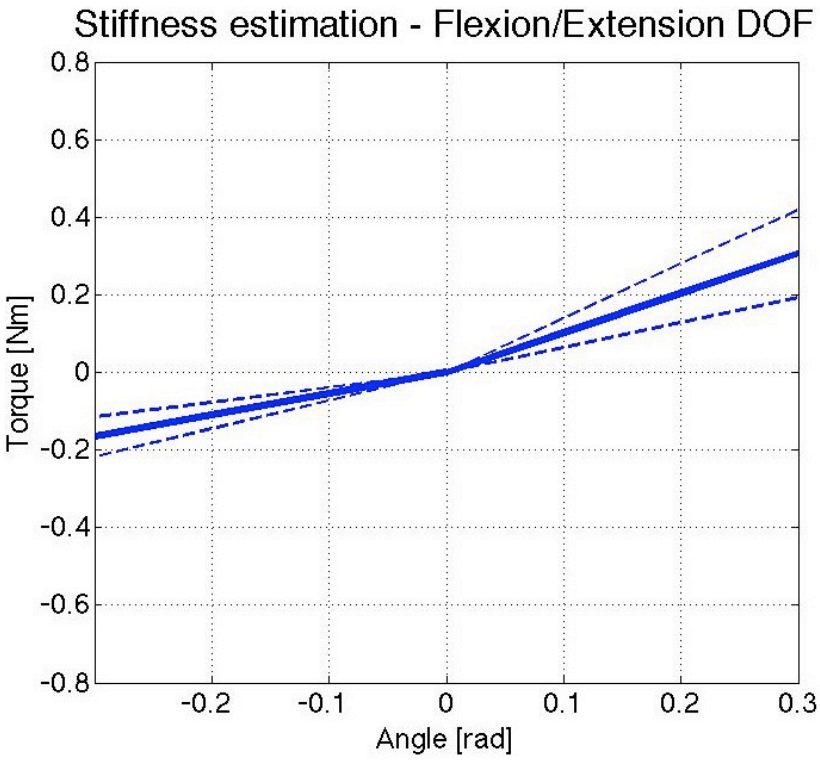

Figure 3.21: Mean stiffness of all subjects, corrected for the hardware bias for flexion/extension DOF; the dashed lines are the curves related to the Mean SD stiffness.

Domenico Formica

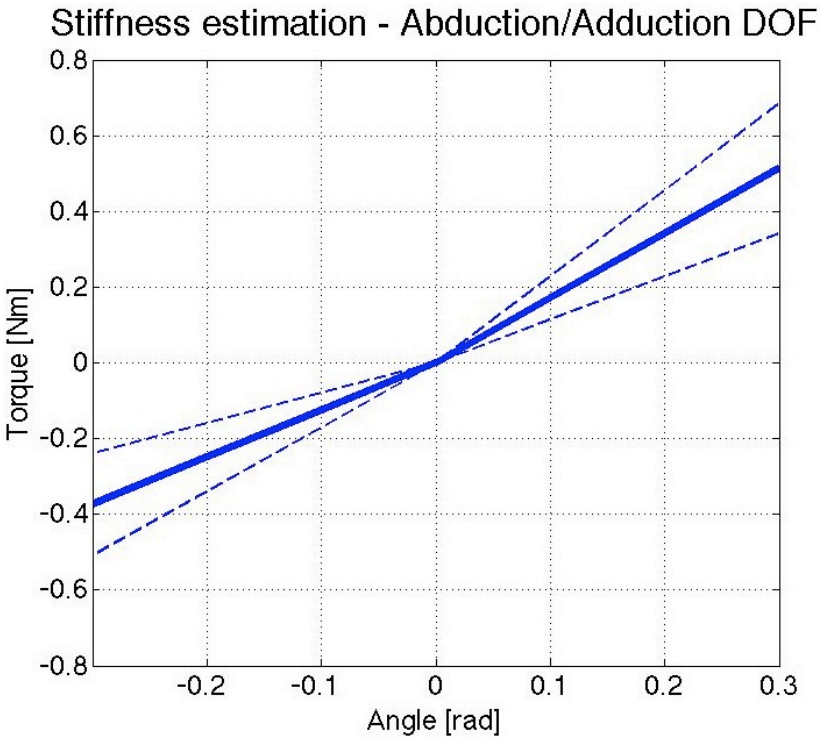

Figure 3.22: Mean stiffness of all subjects, corrected for the hardware bias for abduction/adduction DOF; the dashed lines are the curves related to the Mean SD stiffness.

fig. 3.26).

3.2.4 Discussion

The main goal of this study was to find a reproducible, quantitative method to estimate the passive stiffness of the wrist joint in healthy subjects and pave the way for further studies with subjects with neuromuscular disorders. The results presented in table 1 showed that differences between stiffness in flexed and extended position, as well as abducted and adducted were highly significant in unimpaired subjects (α=0.05, FE and AA: $p < 0.01$), while the PS stiffness

Domenico Formica

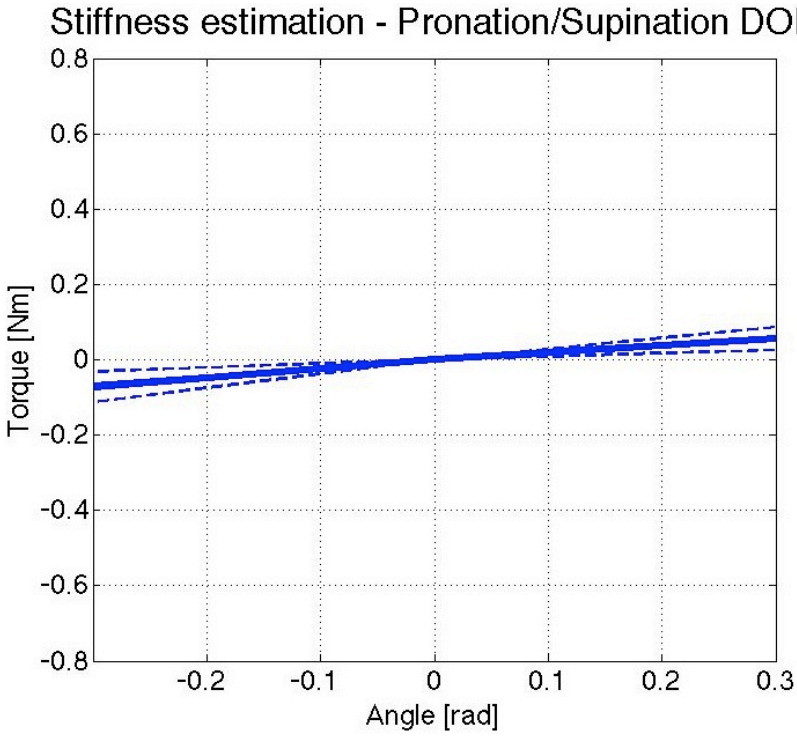

Figure 3.23: Mean stiffness of all subjects, corrected for the hardware bias for pronation/supination DOF; the dashed lines are the curves related to the Mean SD stiffness.

Table 3.2: Mean stiffness estimates from all subjects ± SD, corrected for the hardware bias (the values in the Mean stiffness column are already corrected for the hardware bias).

Position	Mean stiffness [Nm/rad]	Hardware bias correction [Nm/rad]
Flexed	0.554 ± 0.170	0.142 ± 0.022
Extended	1.021 ± 0.379	0.146 ± 0.093
Abducted	1.710 ± 0.573	-0.089 ± 0.059
Adducted	1.245 ± 0.448	-0.024 ± 0.057
Pronated	0.183 ± 0.135	0.415 ± 0.046
Supinated	0.224 ± 0.101	0.357 ± 0.063

Domenico Formica

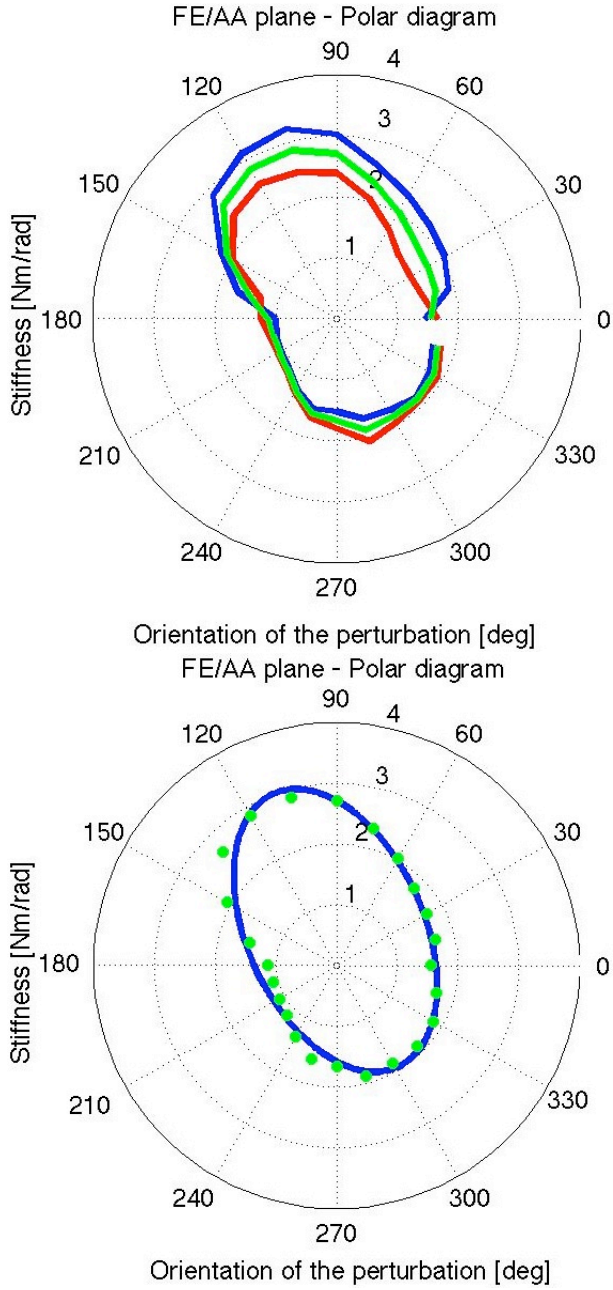

Figure 3.24: An example of combined FE/AA stiffness for one subject calculated using the fitting ellipse method. A: Values of stiffness in the 24 direction for the OUTBOUND movements (blue line), INBOUND movement (red line) and the mean values for each direction (green line). B: Fitting of the 24 mean stiffness values (the dots in the plot) with an ellipse (solid line).

Domenico Formica

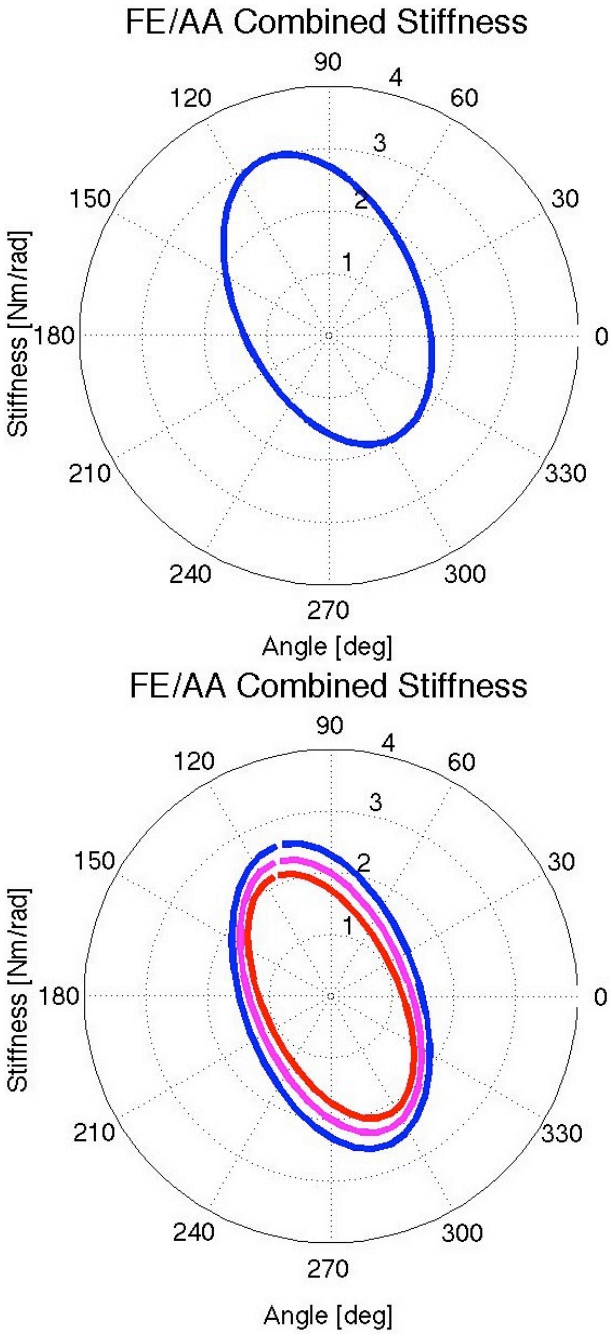

Figure 3.25: An example of the stiffness ellipses of one subject calculated using the fitting ellipse method (A) and the multivariable linear regression (B). In B are reported the ellipse for the OUTBOUND (blue line), INBOUND (red line) and total regression (pink line).

Domenico Formica

Table 3.3: Mean stiffness ellipse parameters from all subjects ± SD, calculated using the fitting ellipse method and the multivariable linear regression.

Estimation method	Magnitude [Nm/rad]^2	Eccentricity	Tilt [deg]	CURL [Nm/rad]	$\det(K_a)/\det(K_{tot})$
Fitting ellipse method	8.16 ± 3.67	0.72 ± 0.12	23.6 ± 15.2		
INBOUND regression	5.85 ± 2.99	0.64 ± 0.14	26.0 ± 10.6	0.06 ± 0.09	0.002 ± 0.005
OUTBOUND regression	8.78 ± 3.92	0.68 ± 0.14	16.2 ± 8.8	-0.14 ± 0.11	0.003 ± 0.004
COMPOSITE regression	8.27 ± 3.17	0.73 ± 0.13	25.8 ± 9.2	-0.03 ± 0.09	0.001 ± 0.002

appears to be quite symmetrical and the stiffness values are much lower than the two other DOFs. A plausible explanation for this difference is given by Gonzalez et al. [110], when assuming that passive resistance to stretching of the muscles is a main contributor to joint impedance. The summed physiologic cross-sectional area (SPCA) of the flexors is approximately twice the one of the extensors, implicating that more muscle volume has to be lengthened during passive extension than during flexion. Furthermore, the mean moment arm of the flexors is 23 % larger. Findings of Delp et al. [111] confirm significant differences between maximum voluntary torques on both sides of the neutral position for FE, but also for AA. A proportional relation between maximum voluntary torque and SPCA would mean a larger SPCA for adductors as opposed to abductors. We found no studies for the PS degree of freedom. Table 3.3 shows the results using the stiffness ellipses, which capture the main geometrical features of the elastic force field through three parameters: magnitude (the area), shape (the ratio of the axis) and orientation (direction of the major axis). The magnitude of the ellipses, that represents overall strength of the elastic field, is the only parameter showing a rather high intra- and inter-subject variability. Shape and orientation of the stiffness field seem to be quite invariant across different subjects with anisotropy of 0.7 (ratio between minor and major axis) and confirm the results of the 1-D protocol. The most novel result relates to the evaluation of the conservative and non-conservative components of the stiffness. The curls of the stiffness matrix, that quantifies the amount of non-conservative energy dissipated to move the wrist along a closed path, were found to be close to zero. The conservative part of the stiffness

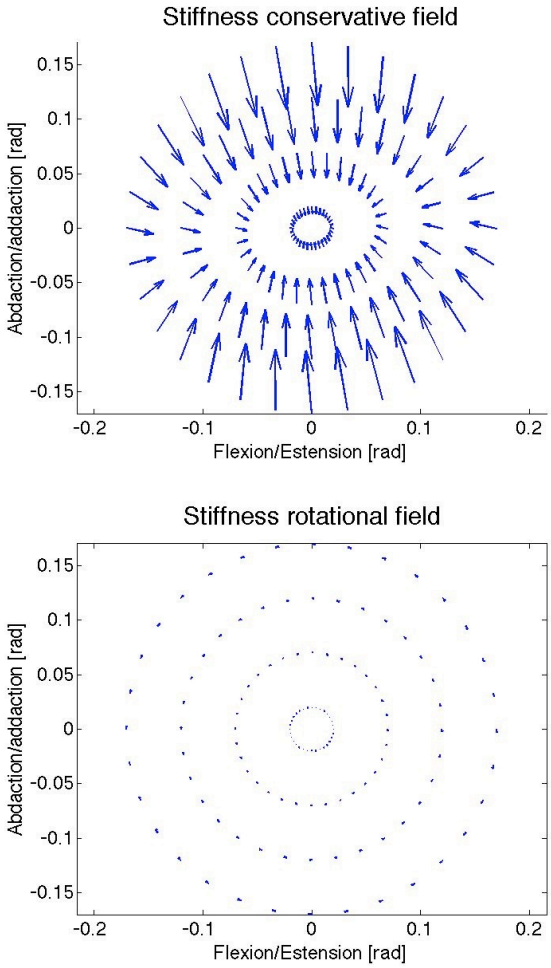

Figure 3.26: Passive Stiffness Matrix for the Wrist. The left plot shows graphically the magnitude of the conservative component of the wrist, while the right plot shows the much smaller non-conservative component.

Domenico Formica

matrix was found to account for over 99 % of the overall matrix. These results show that the neuromuscular system of the wrist joint is predominantly spring-like; this characteristic of the neuromuscular system has been demonstrated earlier for the other human joints of the upper limb [32], but to our knowledge, it has never been demonstrated for the wrist joint. We determined for the first time that similarly to the arm and forearm, the wrist joint exhibits a spring-like behavior.

Domenico Formica

Chapter 4

BIOINSPIRED INTERACTION CONTROL FOR ROBOT-AIDED MOTOR THERAPY

In this chapter a new control approach is proposed to manage interaction in robot-mediated motor therapy of the upper limb, that is purposively conceived for this application field. The control law has been named *torque-dependent compliance control in the joint space* and its applicability to robot-aided motor therapy has been validated in comparison with another bioinspired interaction control previously presented in literature, the *coactivation-based compliance control law*.

4.1 Introduction

Robotic systems for robot-aided neuro-rehabilitation always operate in tight physical contact with the user. This entails that in the scenario of automatic control developed for robotics, the strategies which best fit machines for neurorehabilitation are interaction controls with a direct or indirect regulation of the force exerted in the interaction. In the history of control, the main approaches to the interaction control appeared at the first 70s and were basically focused on assembly and part mating tasks. Many solutions were conceived for this kind of application, still successfully applied. They vary from

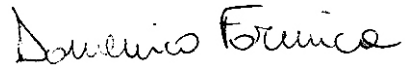

the concept of active compliance [112, 113] to the concept of impedance control [114, 115, 116], up to the hybrid position/force control [117]. Nowadays they still represent milestones of interaction control. However, they often need to be re-examined because of the working environment is getting more and more complex and industrial tasks can be hardly regarded as a set of repetitive and pre-defined motor actions [118]. Moreover, introducing robotic machines in application fields different from industry, like rehabilitation robotics, requires accounting for fundamental parameters in the control, such as the variability of the workspace, safety in the physical interaction, robot adaptability, thus implying reformulating and heavily re-visiting traditional interaction control laws.

The standard control strategies cant completely address the requirements of the rehabilitation context. The main reason is that, in the rehabilitation motor therapy field, the strict interaction between the patient and the machine is not an occasional event, as in several industrial applications, but is the main requirement. The working environment of a robotic machine for motor therapy can be regarded as partially unstructured. In fact, interaction conditions between the robot and the patient can notably vary depending on the residual motor capabilities of patients and their unpredictable reactions to the therapeutic simulations [2]. For these reasons the control system of robotic machines for motor therapy is required to be highly adaptable and safe. In particular, the robot control system has to ensure a high level of adaptability to the different motor capabilities of the patients, different for each patient, and to devote maximum priority to safety in the interaction, also at the expense of the accuracy in the execution of the motor task. Furthermore, an ideal control system for robot-mediated motor therapy, has to be portable, so to be easily instantiated on different types of rehabilitation machines, i.e., operational rehabilitation machines or else exoskeletal rehabilitation machines [56, 119], still providing similar therapeutic performance by just readapting few parameters of the control law. Finally, a good level of flexibility is needed for the machine to be prone to implement different motor tasks, with various kinematic and dynamic characteristics as required by different clinical research protocols. In particular, studies on the typical tasks of rehabilitation motor therapy have shown that, in view of the differences in the patient residual motor capabilities, at least three different operating modalities can be listed which the control has to be able to implement [120]:

- Passive Mode: the patient is unable to autonomously accomplish the motor task and the robot actively drives his/her limb. The trajectory is

fully determined by the robot control system, unless the patients opposes a resistance to motion which exceeds safety specifications.

- Active-Assisted Mode: the patient starts moving but he/ she is unable to reach the target; the robot helps him/her complete the programmed task. When the robot takes control of the task, it goes to passive mode. Initially the machine is fully compliant to human motion, until it stops.

- Active-Constrained Mode: the patient is able to complete the movement, and the robot can exert a set of programmed force fields to allow a complete recovery of the muscular tone. Here, the trajectory of the end effectors dynamically depends on the interaction between the robot and the human arm.

Traditional interaction control schemes are typically used to control rehabilitation robotic machines and manage interaction with the patient. For instance, impedance control [114] is successfully used in motor therapy [37], since it allows finely regulating the mechanical impedance of robots interacting with an unstructured environment. It is basically thought for interaction in the Cartesian space and, consequently, is especially applicable to operational machines. Further, impedance control requires an accurate knowledge of the dynamic parameters of the robotic system, in order to compensate robot dynamics. This increases difficulties in implementing the control law and entails computational burden which may limit the field of application of this powerful technique.

This chapter proposes a new control approach to manage interaction in robot-mediated motor therapy of the upper limb, that is purposively conceived for this application field. The control strategy tries to pave the way for developing control solutions able to answer the requirements of adaptability, safety, portability, and flexibility by proposing a compliant control in the joint space, which is computationally simple with respect to other traditional approaches and potentially applicable to operational as well as exoskeletal machines.

The control law has been named torque-dependent compliance control in the joint space. It originates from the analysis of the basic operating modalities of the rehabilitation motor therapy and, also, from the study on the fundamental mechanisms of biological motor control for generating planar movements and on viscoelastic regulation in the human arm [32, 121, 122, 123, 102, 124]. With reference to the biological motor control, the torquedependent compliance control law in the joint space tries to mimic the action of the central nervous system in regulating elastic properties of a human arm. In particular,

Domenico Formica

relations between the torques exerted by the muscles and the joint stiffness are examined and approximately replicated, for implementing an effective low level compliance control loop. At a higher level, interaction control between patient and robot is achieved by a traditional direct force control law [125].

The design of new interaction controls that are bio-inspired (i.e. the way the machine regulate the interaction with the environment, in this case the patient, is borrowed to the biological motor control) has been successfully used in several previous studies. For example, the same bio-inspired approach led to the formulation of the *self-adaptive compliance control law* [126] and the *coactivation-based compliance control* [127]. In particular, the *torque-dependent compliance control in the joint space* presented here, has been tested and validated in comparison with the *coactivation-based compliance control law*. For this reason a brief description of the *coactivation-based compliance control law* is reported in Section 4.2. In Section 4.3 the theoretical formulation of the *torque-dependent compliance control in the joint space* is presented. Then, in Section 4.4 a comparative validation of basic adaptability and safety requirements of the two control schemes is carried out in simple and ordinary tasks, such as reaching and contact/noncontact transitions. The comparative analysis is performed in simulation tests, by means of a simulation tool purposively developed in MATLAB/Simulink for modeling interaction, and in experimental trials on an 8 degree-of-freedom (i.e. dof) robot arm. The preliminary experimental tests are reported to demonstrate the feasibility of using the proposed approach for guaranteeing safe interaction with the patient. Finally, Section 4.5 reports results of simulation tests of interaction between an operational machine and a patient in a plane during motor therapy. The dynamics of the MIT-Manus rehabilitation robotic machine [37] is modelled as coupled with the dynamics of the human arm and a set of incorrect movements of the patient is simulated through the developed simulation tool to test the control capability of counterbalancing a pathological behaviour.

4.2 State of the art: Coactivation-based compliance control in the joint space

In this chapter the *coactivation-based compliance control in the joint space* [127] has been used as benchmark for the evaluation of the performance of the new proposed bio-inspired controller, i.e. the *torque-dependent compliance control in the joint space*.

The Coactivation-based control borrows from biology the term coactiva-

tion, that is the biological mechanism responsible for the regulation of the arm viscoelastic properties at the level of muscles and joints, and indirectly at the level of end effector [128, 129, 130]. Moreover, in [128] it is proposed that in the human arm feedback acts in the interaction control by regulating the muscular activity in accordance with the movement error.

The *coactivation-based compliance control in the joint space* is formulated as follows [127]:

$$\tau = K_P(c)\tilde{q} - K_D(c)\dot{q} + g(q) \tag{4.1}$$

where $g(q)$ is the estimate of the gravitational torques acting on the joints, and stiffness and damping matrices K_P and K_D are linear functions of a unique parameter c, called *coactivation* by analogy with the biological mechanism. An appropriate choice for the c function allows improving arm accuracy in free space, by increasing stiffness, and increase arm compliance and elasticity in constrained space, by decreasing stiffness when an external bound is sensed. In both cases, the gains of diagonal matrices K_P and K_D evolve from an initial value, experimentally evaluated, as a function of a unique factor, that is the coactivation.

In the free space, the i-th element of K_P increases from its minimum value as

$$k_P(c) = \begin{cases} k_{Pmin} & \text{if } c = 0 \\ k_{Pmin} + \bar{k}_p c & \text{if } c \neq 0, \quad k_P < k_{Pmax} \\ k_{Pmax} & \text{if } c \neq 0, \quad k_P \geq k_{Pmax} \end{cases} \tag{4.2}$$

where the coefficient $\bar{k}_p$ can be different for each joint, in order to allow regulating the level of coactivation for each of them. In (4.2), k_{Pmin} is the minimum gain allowing a quite accurate motion and k_{Pmax} is the maximum gain which still ensures stability in the motion. The updating law for c is an increasing monotonic function of the sole position error, i.e.

$$c = \beta\sqrt{\tilde{q}^T\tilde{q}} \tag{4.3}$$

as presented in [128] for the human visco-elastic regulation. In (4.3), β is a positive coefficient. An analogous adaptable law is proposed for the viscosity parameters. The i-th element of K_D matrix evolves over time like (4.2), but with a slower increasing rate, i.e.,

$$k_D(c) = \begin{cases} k_{Dmin} & \text{if } c = 0 \\ k_{Dmin} + \bar{k}_d c & \text{if } c \neq 0, \quad k_D < k_{Dmax} \\ k_{Dmax} & \text{if } c \neq 0, \quad k_D \geq k_{Dmax} \end{cases} \tag{4.4}$$

Domenico Formica

In the constrained space, k_P function decreases from its initial value k_{Pin} with a law similar to the free space, i.e.

$$k_P(c) = k_{Pin}\bar{h}c \tag{4.5}$$

$$c = c_{min} + \alpha\frac{1}{\sqrt{f^T f}} \quad \text{if} \quad f^T f \neq 0 \tag{4.6}$$

where $k_{Pin}\bar{h}$ is the maximum value for the proportional parameter, and $\bar{h}$ is a scalar coefficient playing the same role of $\bar{k}_p$. The viscosity parameters k_D in constrained motion observe the same law as in (4.5).

The block scheme of the *coactivation-based compliance control in the joint space* is reported in Fig. 4.1.

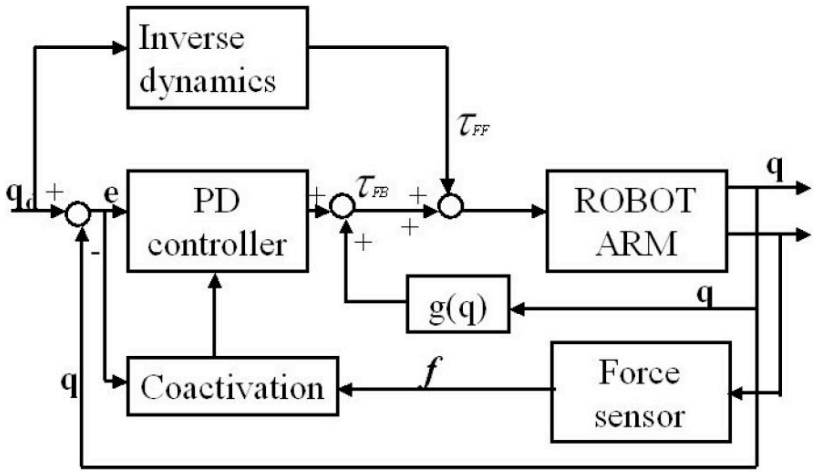

Figure 4.1: Block scheme of the coactivation-based compliance control.

4.3 Torque-dependent compliance control in the joint space

As the *coactivation-based compliance control in the joint space*, the control law proposed in this chapter is deeply bio-inspired. The biological motor control for the visco-elastic regulation in voluntary arm movements is assumed as reference

Domenico Formica

and the robot behavior in the free space as well as in the constrained space is regulated.

As already explained in [126], [127], the choice of designing an interaction control based on the compliance regulation at the level of joint space is entailed by the following factors. From neurophysiological studies [32, 121, 122, 123, 102, 124] it emerges that visco-elastic regulation in humans is directly achieved at the level of muscles and joints and indirectly at the level of end effector. On the other hand, from a robot control viewpoint, implementing a control in the joint space does not require to enter details of robot dynamics, thus allowing reducing the computational burden and extending the approach to different mechanics. This imply that in applications of rehabilitation motor therapy a control in the joint space can be easily applied to operational as well as exoskeletal machines (i.e. portability).

The new bio-inspired control proposed here, namely the torque-dependent compliance control in the joint space, tries to replicate results obtained in [102] on human subjects, where joint stiffness is demonstrated to be strictly dependent on the torques exerted by the muscles on the joints. In fact, joint stiffness seems to increase as the torque module raises and in [102] authors underline that the relation between joint stiffness and torque module can be assumed linear, as shown in Fig. 4.2 extracted from [102].

The torque-dependent compliance control in the joint space is a parallel force/position control where the position control is a compliance control in the joint space based on PD actions. In the free space the PD control tries to replicate results obtained in [102] on human subjects, by making the joint stiffness linearly vary with the torque module as:

$$R_{ij}(\tau_k^m) = \begin{cases} R_{ij}^{min} + k_{ij}|\tau_k^m| & \text{if} \quad R_{ij} < R_{ij}^{max} \\ R_{ij}^{max} & \text{if} \quad R_{ij} \geq R_{ij}^{max} \end{cases} \tag{4.7}$$

where $i, j, k = \{e, s\}$, being subscripts e and s the elbow and shoulder joint, respectively. The corresponding stiffness matrix is:

$$R(\tau^m) = \begin{bmatrix} R_{ss}(\tau_s^m) & R_{se}(\tau_e^m) \\ R_{es}(\tau_e^m) & R_{ee}(\tau_e^m) \end{bmatrix}. \tag{4.8}$$

Note that a maximum value R_{ij}^{max} for each joint needs to be imposed in order to avoid instability in the control. As regards damping matrix D, it is assumed to be constant since in [102] the variation of viscosity with joint torques seems to be negligible. Definitely, in the free space robot behavior is regulated by the following control law:

Domenico Formica

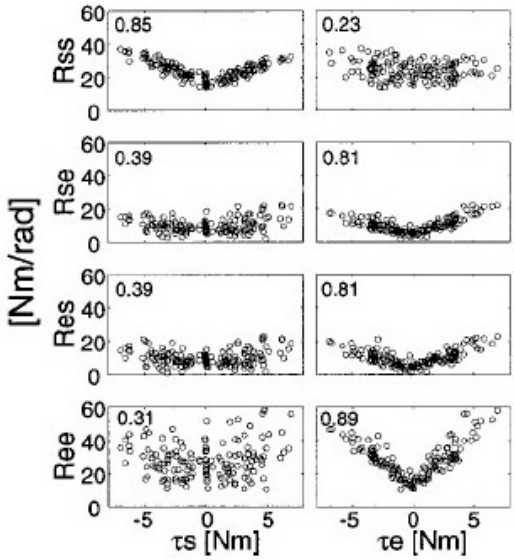

Figure 4.2: Joint torque and joint stiffness relationships for one subject (extracted by [102]).

$$\tau = R(\tau^m)\tilde{q} - D\dot{q} + g(q) \tag{4.9}$$

where $R(\tau^m)$ is expressed by (4.7) and (4.8).

For the robot behaviour in the interaction with the human subject, the traditional approach to force control [125] is used. This is because the control is thought to be applied to motor therapy, where the three modalities of passive mode, active assisted mode and active constrained mode are to be performed. Thus, the basic idea for the control in the interaction with a patient is that the therapist is capable of guiding, assisting or forcing the subject in the execution of the motor task. Control in the constrained space is then based on a force feedback loop which, in addition to a position loop, makes the robot capable of changing the desired trajectory depending on the force error (Fig. 4.3).

The desired trajectory the robot has to follow in the Cartesian space is composed of two terms:

$$x_d = x_{dp} + x_F \tag{4.10}$$

Domenico Formica

where x_{dp} is the desired trajectory in absence of interaction, and x_F determines the displacement from x_{dp} depending on the force error as follows:

$$x_F = K_{FP}(F_d - F) + K_{FI}\int_0^t (F_d - F)d\varsigma. \tag{4.11}$$

In (4.11) K_{FP} and K_{FI} are the proportional and integral matrix gains of the force control and F_d is the reference force vector imposed by the therapist on the base of the degree of disability of the patient.

The block scheme of the torque-dependent compliance control in the joint space is shown in Fig. 4.3.

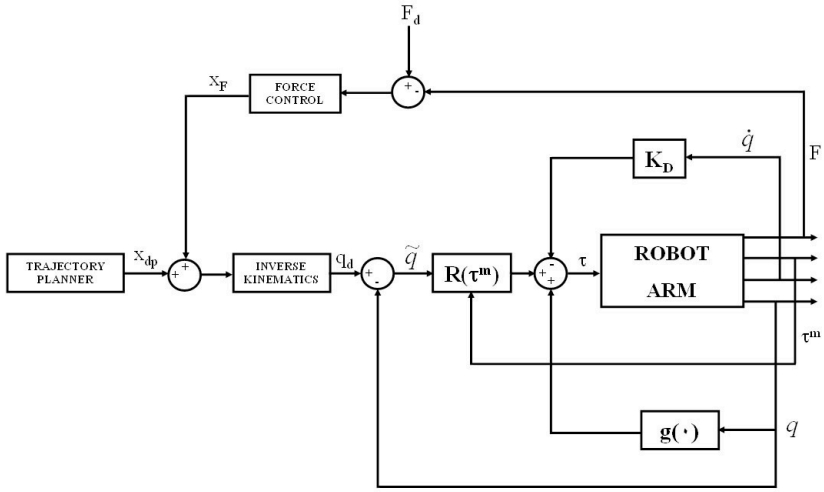

Figure 4.3: Block scheme of the torque-dependent compliance control.

4.4 Comparative control analysis

4.4.1 Description of the simulation tool

A simulator has been developed in MATLAB/Simulink for a preliminary validation and a comparative analysis of the control laws (4.1) and (4.9). The simulator models a 2-dof robot arm interacting with a human arm [131, 132]. The simulated robot arm is the 2-dof MIT-Manus operational robotic machine

Domenico Formica

(see Fig. 4.4). The main reason for the choice of the MIT-Manus system is that it is a commercial robot specifically designed for robot-aided rehabilitation and tested in several clinical studies of motor therapy [37, 133, 134, 39]. The model developed in MATLAB/Simulink is based on kinematic and dynamic parameters extracted from [135]. On the other hand, for the human arm a simplified planar model has been considered, consisting of two joints (a shoulder and an elbow), two links and three couples of muscles (see Fig. 4.4) [122]. This type of simplified model is widely used in most neurophysiological studies regarding human motor control [114, 136].

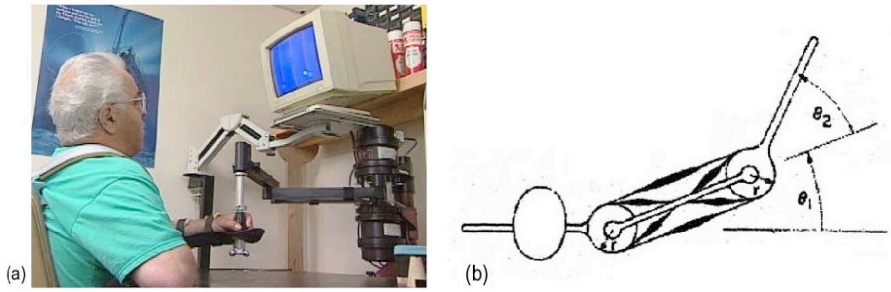

Figure 4.4: The MIT-MANUS rehabilitation robot (a), and a planar model of the human arm (b).

The dynamic model of the MIT-MANUS robot can be described as:

$$B_{ROB}(q)\ddot{q} + C_{ROB}(q,\dot{q})\dot{q} = \tau - J^T_{ROB}(q)F_{ROB}. \tag{4.12}$$

whereas the dynamics of the human arm interacting with the robot can be expressed as:

$$B_{HUM}(\theta)\ddot{\theta} + C_{HUM}(\theta,\dot{\theta})\dot{\theta} = \tau_{HUM} - J^T_{HUM}(\theta)F_{HUM}. \tag{4.13}$$

In (4.12) and (4.13),

- q, $\dot{q}$, $\ddot{q} \in R^{2\times 1}$ are the robot joint position, velocity and acceleration vectors, respectively;
- $B(q) \in R^{2\times 2}$ is the joint inertia matrix;
- $C(q,\dot{q})\dot{q} \in R^{2\times 1}$ is the vector of centrifugal and Coriolis torques;

Domenico Formica

- $J(q) \in R^{2\times 2}$ is the robot Jacobian matrix;
- $\tau \in R^{2\times 1}$ is the torque vector;
- $F \in R^{2\times 1}$ is the vector of forces exerted on the external environment.

and subscripts ROB and HUM indicate that the quantities are referred to the MIT-MANUS and the human arm, respectively.
The values of matrices $B_{ROB}(q)$, $C_{ROB}(q,\dot{q})$, $J_{ROB}(q)$ are taken from [135], while the values of $B_{HUM}(\theta)$, $C_{HUM}(\theta,\dot{\theta})$, $J_{HUM}(\theta)$ are based on the anthropometric data in [121].

Furthermore, in view of the physical interaction between the two systems, forces F_{ROB} and F_{HUM} are equal and opposite in sign (i.e. $F_{ROB} = -F_{HUM}$) while position, velocity and acceleration in the Cartesian space are the same. The inequality in the Cartesian space yields:

$$\theta = k_{HUM}^{-1}(k_{ROB}(q)) \tag{4.14}$$

$$\dot{\theta} = J_{HUM}^{-1}(\theta) J_{ROB}(q)\dot{q} \tag{4.15}$$

$$\ddot{\theta} = J_{HUM}^{-1}(\theta)(\dot{J}_{ROB}(q)\dot{q} + J_{ROB}(q)\ddot{q} - \dot{J}_{HUM}(\theta)\dot{\theta}) \tag{4.16}$$

where $k_{ROB}(q)$ is the robot forward kinematics and k_{HUM}^{-1} is the inverse kinematics of the human arm. Thus, the joint variables for the human arm (i.e. $\ddot{\theta}$, $\dot{\theta}$, θ) can be calculated as a function of the MIT-MANUS joint variables (i.e. $\ddot{q}$, $\dot{q}$, q).

By substituting Eqs. (4.14)–(4.16) in (4.13) and extracting $F_{HUM} = -F_{ROB}$, a complete dynamic model of the interacting robot-human system can be obtained by Eq. (4.12).

In Fig. 4.5 the image of the two simulated interacting systems is shown. The MIT-Manus system is represented in blue while the human arm is in red. The handle of the robot where the patient is attached is coloured in pink.

Control torques τ_{MIT} for the robotic system are provided by the robot control law.

For the human arm (4.13), instead, motor torques τ_{HUM} are generated by the motor commands from the CNS [121], [122], [99], [136] and are dependent on the visco-elastic muscle behavior. Here, for simplicity, human muscular activity is not modeled and only the consequence at level of joints is considered. This entails a joint visco-elastic behavior described as:

$$\tau_{HUM} = R_{HUM}(\theta_d - \theta) - D_{HUM}\dot{\theta} \tag{4.17}$$

Domenico Formica

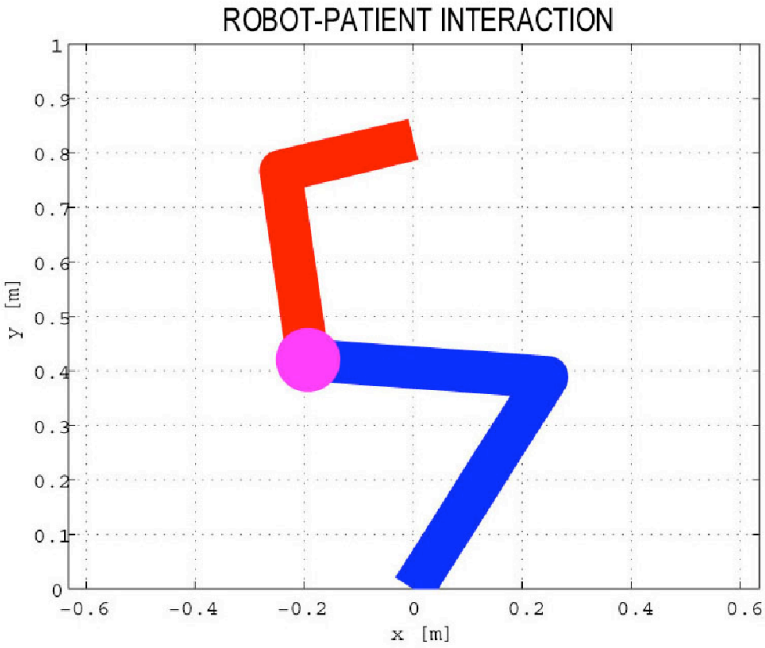

Figure 4.5: Graphical interface of an operational robotic machine interacting with a human subject: the MIT-Manus robot arm is drawn in blue, the human arm is drawn in red

where the values of joint stiffness matrix R_{HUM} and damping matrix D_{HUM} have been chosen in accordance with the data in [102] on the joint visco-elastic behavior of the human arm. Vector θ_d is the arm desired trajectory in the joint space.

4.4.2 Simulation results

Performance of the coactivation-based compliance control in the joint space and of the torque-dependent compliance control in the joint space have been preliminarily compared through the developed simulation tool. The robot arm is regarded as an uncoupled system (i.e., without coupling with the human subject) and is controlled to execute motor tasks of positioning in the free

Domenico Formica

space as well as of interaction with an unexpected constraint.

For the simulation tests in the free space, the robot arm is moved in the Cartesian space from the initial position $P_i = [-0.2; 0.58]$ m to the final position $P_f = [0.2; 0.58]$ m in 4 s plus 2 s for the adjustment. For the control law (4.1) the control gains have been chosen as: $K_{P_{ss}}^{min} = 10.8 \cdot 40$ Nm/rad, $K_{P_{ee}}^{min} = 8.67 \cdot 40$ Nm/rad, $\overline{k}_{P_{ss}} = 2.86 \cdot 40$ Nm/rad, $\overline{k}_{P_{ee}} = 6.82 \cdot 40$ Nm/rad, $K_{D_{ss}}^{min} = K_{D_{ee}}^{min} = 4$ Nm/rad $\cdot$ s^{-1}, $\overline{k}_{D_{ss}} = \overline{k}_{D_{ee}} = 0.1$ Nm/rad $\cdot$ s^{-1}, $\beta = 50$. On the other hand, for the control law (4.9) the visco-elastic parameters have been empirically set as: $R_{ss}^{min} = 10.8 \cdot 40$ Nm/rad, $R_{ee}^{min} = 8.67 \cdot 40$ Nm/rad, $R_{se}^{min} = 2.15 \cdot 40$ Nm/rad, $R_{es}^{min} = 2.34 \cdot 40$ Nm/rad, $k_{ss} = 2.86 \cdot$ rad^{-1}, $k_{ee} = 6.82 \cdot 40$ rad^{-1}, $k_{se} = k_{es} = 7.5 \cdot 40$ rad^{-1}, $K_{D_{ss}} = K_{D_{ee}} = 4$ Nm/rad $\cdot$ s^{-1}. All the parameters have been empirically set, by using as initial values the biological values reported in [102] and changing them to improve performance of the control laws.

The norm of the position error in the Cartesian space for the two cases of *coactivation-based compliance control* and *torque-dependent compliance control* is shown in Figs.. 4.6 and 4.7, respectively. The error time course is very similar and in both cases the maximum value is close to $1.3 \cdot 10^{-3}$ m.

After the analysis in the free space, the effectiveness of the control during interaction in an unstructured environment has been tested. An unexpected external constraint has been simulated and the interaction force between the robot and the constraint has been read. The external constraint has been modeled as an elastically compliant system having stiffness K_e and described by the following equation:

$$F_e = K_e(x_e - x) \tag{4.18}$$

being x_e and x the Cartesian position of the constraint and the robot end effector, respectively, and $K_e = 10^4$ N/m in the simulation.

The robot is moved from the initial position $Pi = [0.46; 0.44]$ m to the final position $Pf = [0.46; 0.44]$ m, and the obstacle is assumed to be vertically positioned in $xe = 0.2$ m. Figures 4.8 and 4.9 report the interaction force in norm for the two cases of coactivation-based and torque-dependent compliance control. In order to compare force performance, control gains for the two control laws have been tuned to generate the same position error. As evident, the interaction force related to coactivation-based compliance control presents a series of spikes in the contact/non-contact transition phase, which are notably reduced in the force evolution related to (4.9). After the transient, both controllers reach a reasonable force value, that is close to 5N for the controller (4.1) and 1N for the controller (4.9). In the constrained motion, the control gains of the coactivation-based control law in (4.5) and (4.6) are chosen as:

Domenico Formica

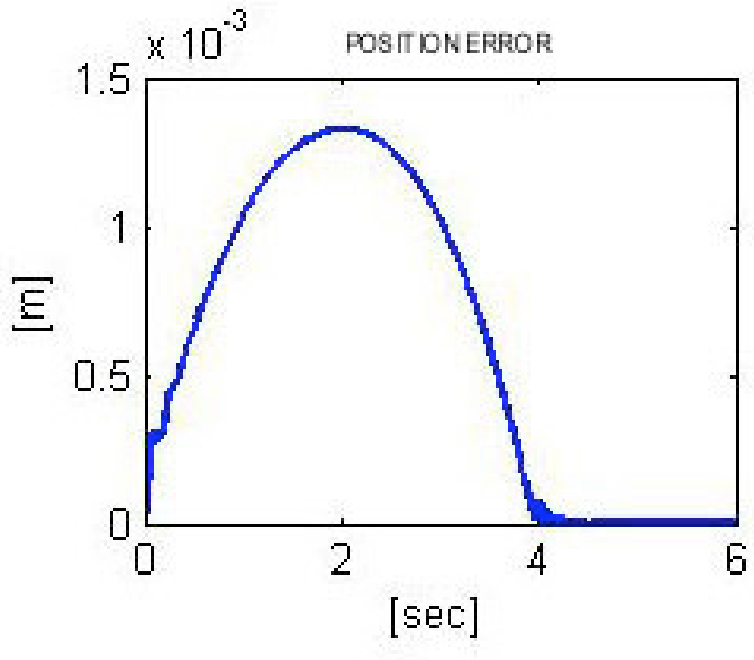

Figure 4.6: Simulation results on position error in the free space for the coactivation-based compliance control law.

$K_{Pin} = diag\{40, 8\}$ Nm/rad, $\overline{H} = diag\{0.8, 0.7\}$, $c_{min} = 0.4$, $\alpha = 1$. For the force control in (4.11) control gains have the following values: $K_{FP} = 10^{-3}$ mN^{-1}, $K_{FI} = 10^{-2}$ m $\cdot$ $(\text{Ns})^{-1}$, $F_d = 1$ N.

4.4.3 Experimental results

Experimental trials of reaching in the free space and motion in the constrained space have been carried out to complete the compared evaluation of the two control laws. The experimental robotic platform consists of the Dexter arm, a robot manipulator at the ARTS Lab of the Scuola Superiore Sant'Anna of Pisa and manufactured by Scienzia Machinale s.r.l. for applications of assistive robotics, and a six-axis ATI force/torque sensor (see Fig. 4.10).

The Dexter arm is made of 8 rotational joints actuated by a mechanical

Domenico Formica

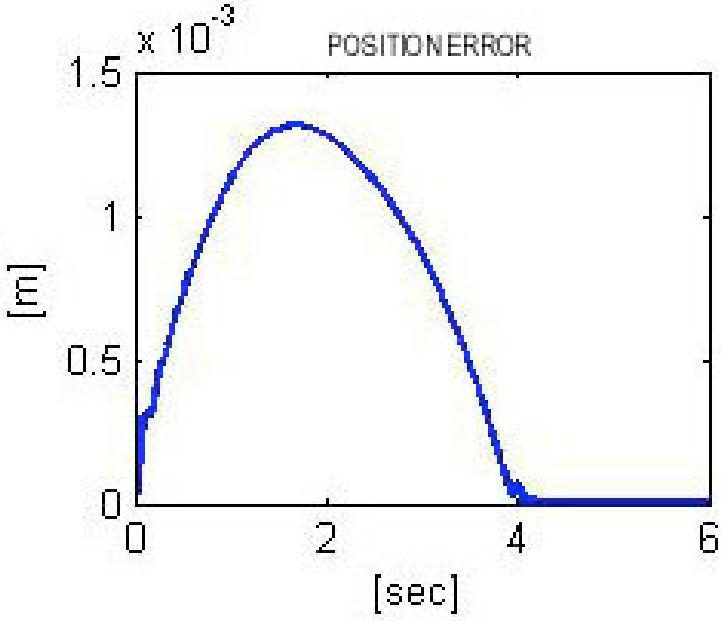

Figure 4.7: Simulation results on position error in the free space for the torque-dependent compliance control law.

transmission system of pulleys and steel cables which determines coupling in the degrees of freedom (see [126] for further details). The force/torque sensor is mounted at the arm wrist and is capable of reading force in the range of $[-210, +210]$N. The sensor is used to monitor force values during interaction and close the loop in the force control. A photo of the experimental setup is shown in Fig. 4.10.

The control law is written in C++ programming language and run on a PC Pentium II under DOS Operating System. The motor commands are sent to the actuation system every 10 ms, by means of two MEI 104/DSP-400 control boards. As in the simulated environment, the experimental tests consist of a series of point-to-point movements in the free space as well as in the constrained space.

For tests in the free space, the Dexter arm is moved in the Cartesian space

Domenico Formica

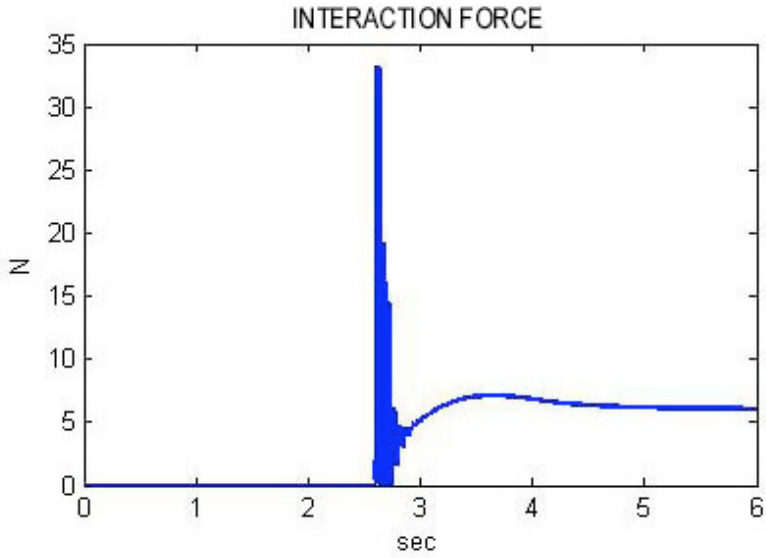

Figure 4.8: Simulation results on interaction force in the constrained motion for the coactivation-based compliance control law.

from the initial position $P_i = [0.70; -0.25; 0.50]$ m to the final position $P_f = [0.50; 0.25; 0.45]$ m in 13 s plus 3 s for the adjustment.. A point-to-point quintic polynomial trajectory (with zero velocity and acceleration boundary conditions) has been planned to guide the robot from the initial to the final configuration. The experimental tests have been performed with high gain values, in order to reach the target position with high precision. Thus, for the *coactivation-based compliance control*, the following values have been chosen: $K_{Pmin} = \text{diag}\{60, 40, 10, 9, 8, 1, 0.2, 0.2\}$, $\beta = 1.5$, $\bar{K}_P = \text{diag}\{3, 2.5, 2.5, 2, 1.8, 1, 0.2, 0.2\}$. Instead, for the *torque-dependent compliance control* R^{min} =diag$\{640, 120, 80, 64, 32, 4, 4\}$ Nm/rad, k =diag$\{20, 20, 16, 14.4, 8, 4, 4\}$ rad^{-1} and K_D=diag$\{10, 10, 6, 2, 2, 0.8, 0.8\}$ Nm/rad $\cdot$ s^{-1} have been set. The position error in the Cartesian space is shown in Figs. 4.11 and 4.12, respectively. Definitely, in the free space performance of the two compliance control laws seems to be comparable.

To evaluate the adaptability of the control laws to unexpected constraints, the robot arm has been commanded to move from the initial position $P_i = [0.50; 0; 0.40]$ m to the final position $P_f = [0.75; 0; 0.40]$ m and the experi-

Domenico Formica

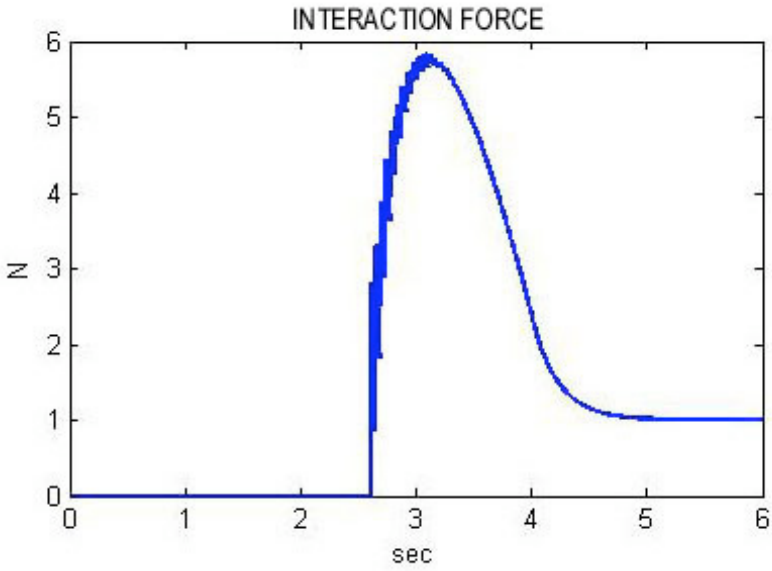

Figure 4.9: Simulation results on interaction force in the constrained motion for the torque-dependent compliance control law.

menter is instructed to constrain the robot end effector by using his/her hand at about $x = 0.60$ m. The results shown in Figs. 4.13, 4.14 correspond to the following set of control parameters: K_{Pin} =diag$\{60, 40, 15, 10, 8, 4, 1, 1\}$ Nm/rad, $\bar{H}$ =diag$\{1, 0.8,$
$0.8, 0.7, 0.7, 0.5, 0.1, 0.1\}$, $c_{min} = 0.4$, $\alpha = 1$ for the control law (4.1) and $K_{FP} = 10^{-3}$ m $\cdot$ N^{-1}, $K_{FI} = 10^{-2}$ m $\cdot$ (Ns)$^{-1}$, $F_{dx} = -5$ N, $F_{dy} = F_{dz} = 0$ N for the control law (4.9). In both cases the robot adapts the trajectory to the external constraint and, for the control (4.9) it also regulates the interaction force to the desired value.

However, it is worth noticing that for the second controller, i.e. the *torque-dependent compliance control*, force time course never resulted in sharp variations at the impact with the constraint, whereas for the *coactivation-based compliance control* force time course appears to be quite impulsive in the adaptation to the obstacle (Fig. 4.13). This achievement is in accordance with results in Figs. 4.9 and 4.8 obtained in the simulation tests and is extremely

Domenico Formica

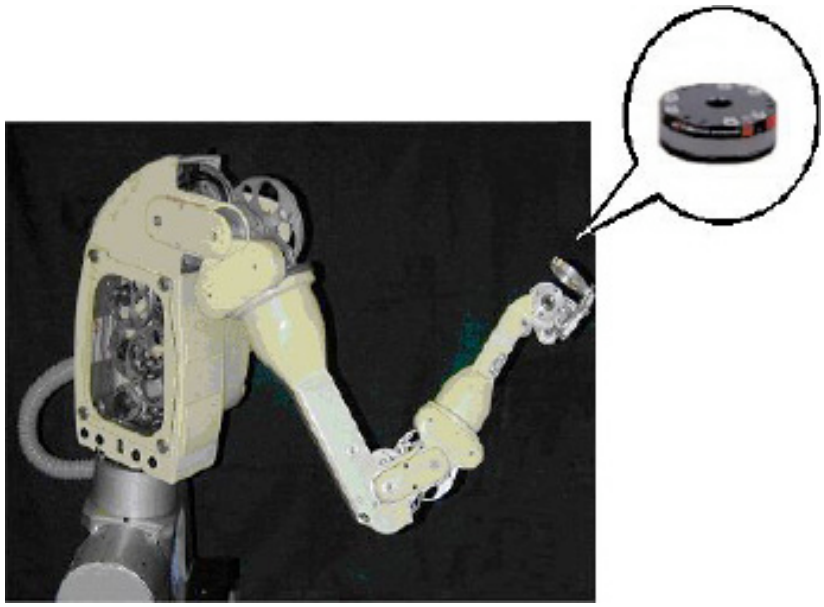

Figure 4.10: The Dexter robot arm with the six-axis ATI force/torque sensor mounted on the arm wrist.

important for selecting the appropriate control law for biomedical applications, where safety and smooth adaptability in the interaction with humans are requirements with maximum priority.

4.5 Simulation tests of human-robot interaction during motor therapy

Following results of comparison between the two control laws, which have shown the torque-dependent compliance control as the safer and more adaptable between the two, an application of (4.9) to interaction with a patient during tasks of motor therapy has been simulated. In particular, through the simulator in Section 4.4.1 three different levels of motor disabilities have been modeled, in order to qualitatively test system adaptability to different interaction conditions. For simplicity, the different pathological levels have been represented by means of sharp deviations of the human arm from the linear reference trajec-

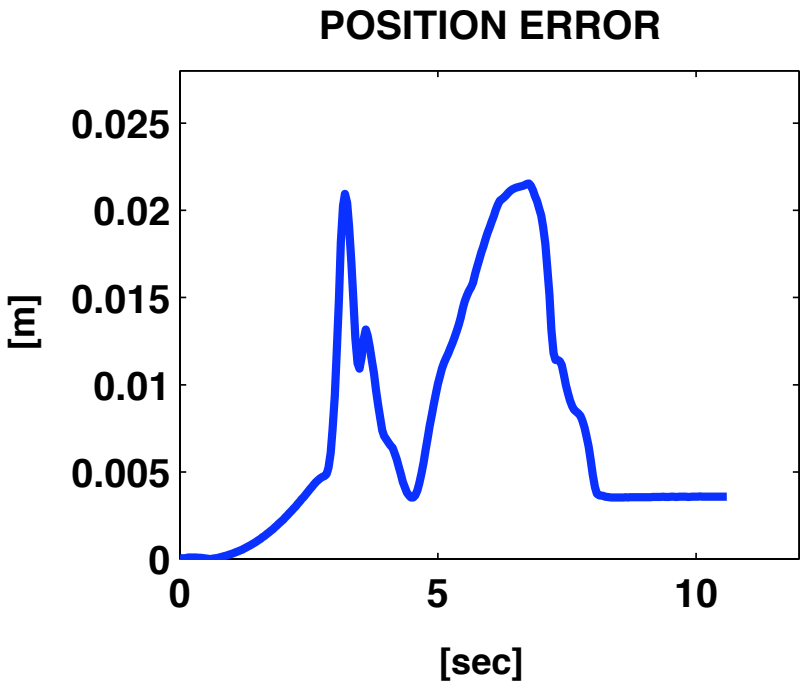

Figure 4.11: Experimental results: norm of the position error in the free space for the coactivation-based compliance control.

tory. Whereas a linear motion from a generic point A to a point B is expected for a healthy subject, a sequence of short linear paths (like a sawtooth function) can be imagined for a patient undergoing neurorehabilitation therapy. The rate of variation of the sawtooth is assumed to be dependent on the level of disability.

The MIT-MANUS robot arm has been controlled to linearly move from the initial point $P_i = [-0.20; 0.42]$ m to the final point $P_f = [0.20; 0.42]$ m in 4 s and force the patient to follow a linear motion in accordance with the level of disability. As natural, the level of robot force has to be opportunely tuned to guarantee safety of operation with human subjects. To this purpose, the reference value for the force control consists of two contributions:

Domenico Formica

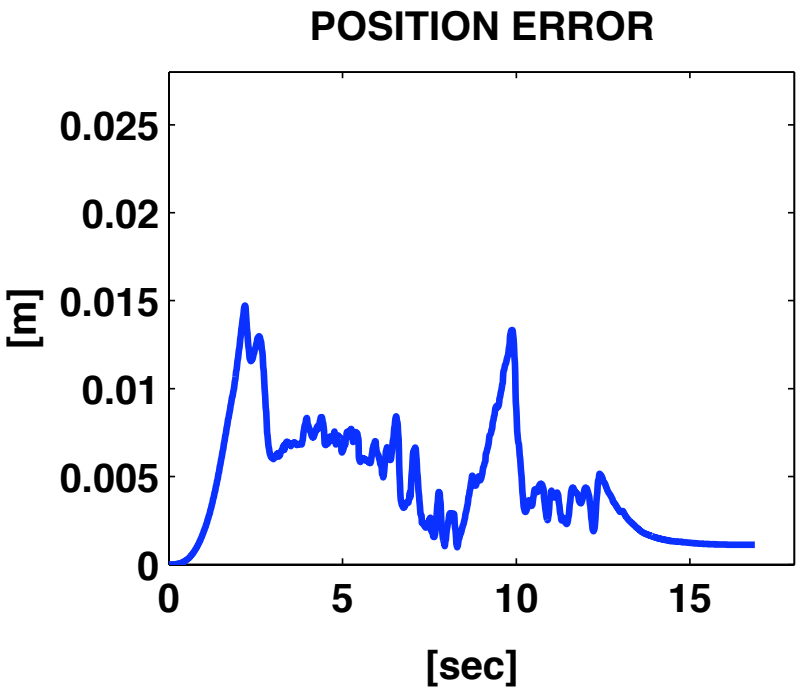

Figure 4.12: Experimental results: norm of the position error in the free space for the torque-dependent compliance control.

- A force $F_{dx} = cost$ that guides the arm in the direction of motion.
- A force perpendicular to the motion direction which counterbalances incorrect movements. It is expressed as $F_{dy} = K_y \tilde{y}$, where $\tilde{y}$ is the position error in the direction perpendicular to the motion and gain K_y assumes higher values as the level of disability increases.

Table 4.5 reports the values of the parameters of the force control used for simulating interaction in the three cases of disability.

For brevity, simulation results only for two levels of disability are reported in this paper. They are shown in Figs. 4.15 and 4.16 and correspond to the simulated case of slight and severe disability, respectively. The two figures show

Domenico Formica

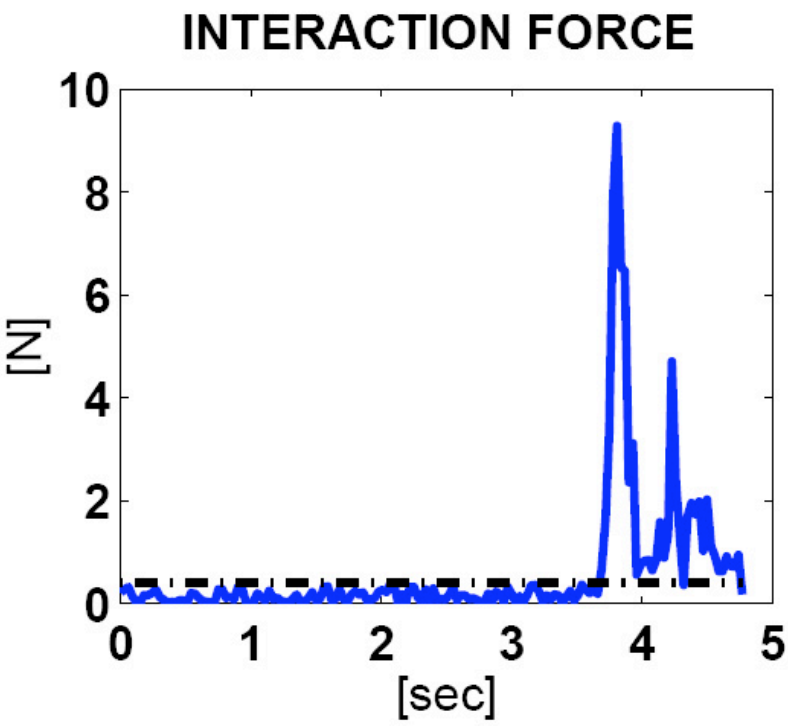

Figure 4.13: Experimental results: interaction force in the constrained motion for the coactivation-based compliance control law.

both the incorrect movement executed by the patient in absence of the MIT-MANUS assistance and the movement described by the patient when guided by the robot. The efficacy of robot corrective actions directly depends on F_{dx} and, especially, on K_y. This is evident also in the case of severe disability in Fig. 4.16. However, it is worth noticing that the choice of the control parameters is superiorly limited due to instability problems and safety in the interaction. High values may determine interaction force that can be dangerous for the patient. For instance, when the critical case of severe disability and high control parameters (F_{dx} = 45 N, K_y = 1000 N/m) has been simulated the interaction force has reached a dangerous peak value of nearby 80 N (see Fig. 4.17). Hence, a superior limit needs to be imposed to the force exerted by

Domenico Formica

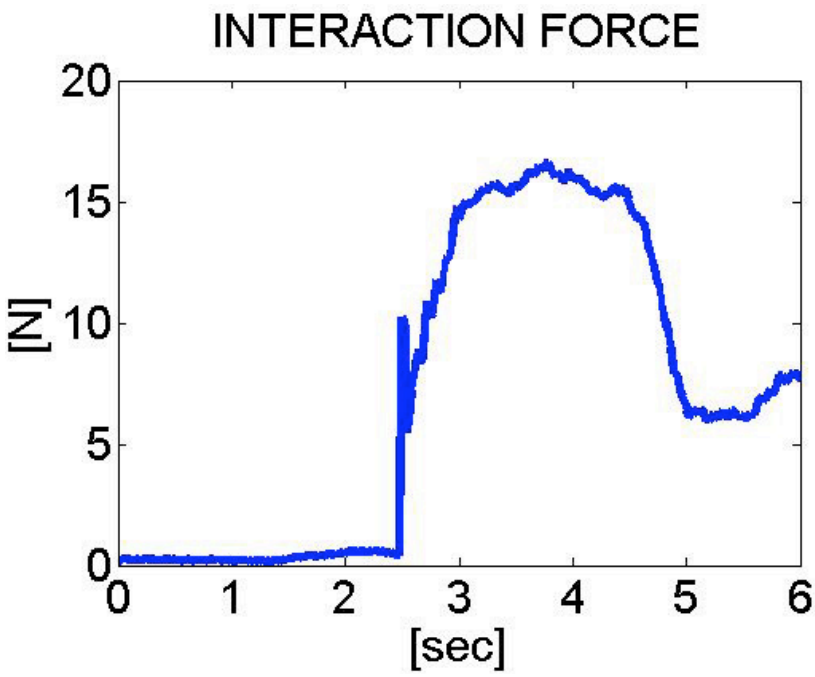

Figure 4.14: Experimental results: interaction force in the constrained motion for the torque-dependent compliance control law.

Disability 1	Disability 2	Disability 3
$F_{dx} = 5$ N $K_y = 100$ N/m	$F_{dx} = 15$ N $K_y = 100$ N/m	$F_{dx} = 30$ N $K_y = 100$ N/m
$F_{dx} = 15$ N $K_y = 100$ N/m	$F_{dx} = 30$ N $K_y = 100$ N/m	$F_{dx} = 45$ N $K_y = 100$ N/m
$F_{dx} = 5$ N $K_y = 1000$ N/m	$F_{dx} = 15$ N $K_y = 1000$ N/m	$F_{dx} = 30$ N $K_y = 1000$ N/m
$F_{dx} = 15$ N $K_y = 1000$ N/m	$F_{dx} = 30$ N $K_y = 1000$ N/m	$F_{dx} = 45$ N $K_y = 1000$ N/m

Table 4.1: Parameters for the force control in the simulation tests of robot interacting with the patient.

Domenico Formica

the robot while guiding the human arm, that is around 45–50 N, as in the real MIT-MANUS system [37].

4.6 Discussion

In this chapter basic criteria for the design and implementation of interaction control of robotic machines for motor therapy have been briefly introduced and a bio-inspired compliance control law developed to address requirements coming from this specific application field have been presented. In particular, a inner-outer control scheme has been designed to ensure a high level of adaptability to different patient motor capabilities and to guarantee a high level of safety in the interaction. Also basic requirements coming from the theory of robot control, such as simplicity of implementation, low computational burden and functional force regulation have been satisfied. The control law, named *torque-dependent compliance control in the joint space* tries to overcome limitations of the traditional interaction control by taking inspiration from biological motor control, and integrates a bio-inspired approach for the low level regulation of robot stiffness with a classical force feedback loop to directly control the interaction with the patient. It basically differs for the strategy of stiffness regulation used to generate a variable proportional gain in the PD control. A preliminary evaluation of the proposed control law has been performed on a simulation tool purposively developed in MATLAB/Simulink. This tool allows simulating the dynamics of the MIT-MANUS rehabilitation robot coupled with a human arm of a patient with different levels of disability. A first set of tests is used to validate the control law with standard techniques; a comparison with the coactivation-based compliance control in [127], used as a reference benchmark to evaluate the performance of the proposed scheme, shows the improvement of the torque-dependent control in situations of contact/non-contact transition. Trials of robot positioning in the free space and in the constrained space have revealed similar performance of the control laws as regards position regulation. However, for force regulation in presence of unexpected constraints the coactivation-based control appears to be less safe than the torque-dependent compliance control, due to the numerous and sharp spikes in the contact/noncontact transitions. This result is enforced by the experimental evidence on a 8-dof robot arm. Following the goodness of performance, an application of the torque-dependent compliance control in the joint space to rehabilitation motor therapy has been simulated. The simulator in fact can be also used to simulate different levels of disability of the patient

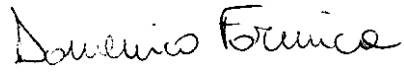

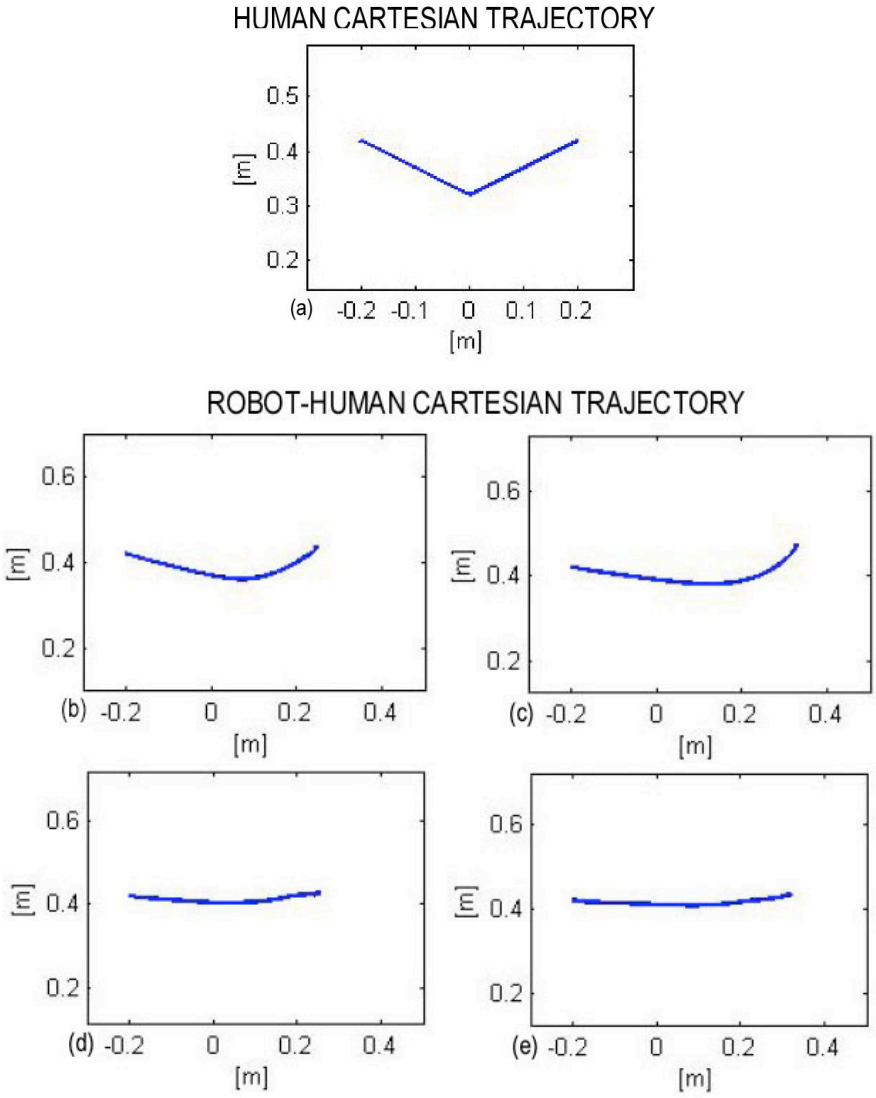

Figure 4.15: Pathological (solid line) and normal (dashed line) trajectories (a) and subject trajectories counterbalanced by the robot for $F_{dx} = 5$ N, $K_y = 100$ N/m (b), $F_{dx} = 15$ N, $K_y = 100$ N/m (c), $F_{dx} = 5$ N, $K_y = 1000$ N/m (d), $F_{dx} = 15$ N, $K_y = 1000$ N/m (e) in case of slight disability.

Domenico Formica

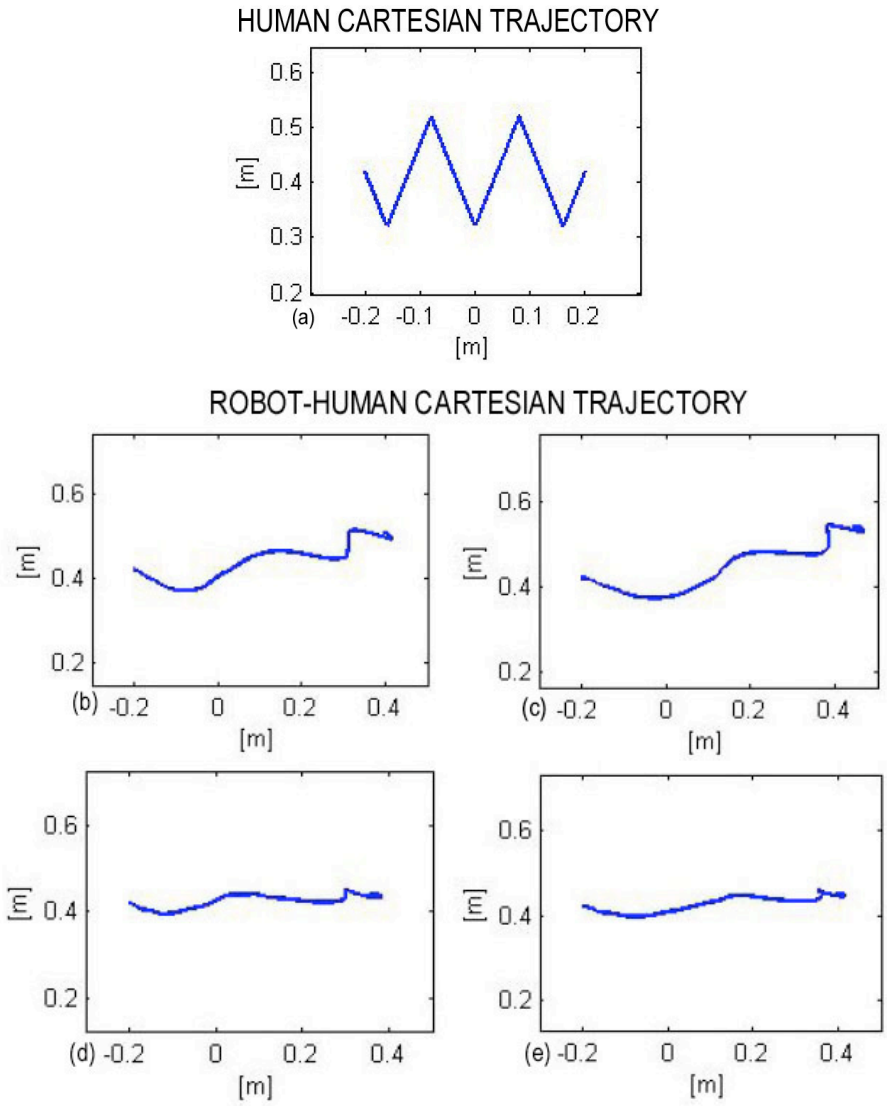

Figure 4.16: Pathological (solid line) and normal (dashed line) trajectories (a) and subject trajectories counterbalanced by the robot for $F_{dx} = 30$ N, $K_y = 100$ N/m (b), $F_{dx} = 45$ N, $K_y = 100$ N/m (c), $F_{dx} = 30$ N, $K_y = 1000$ N/m (d), $F_{dx} = 45$ N, $K_y = 1000$ N/m (e) in case of severe disability.

Domenico Formica

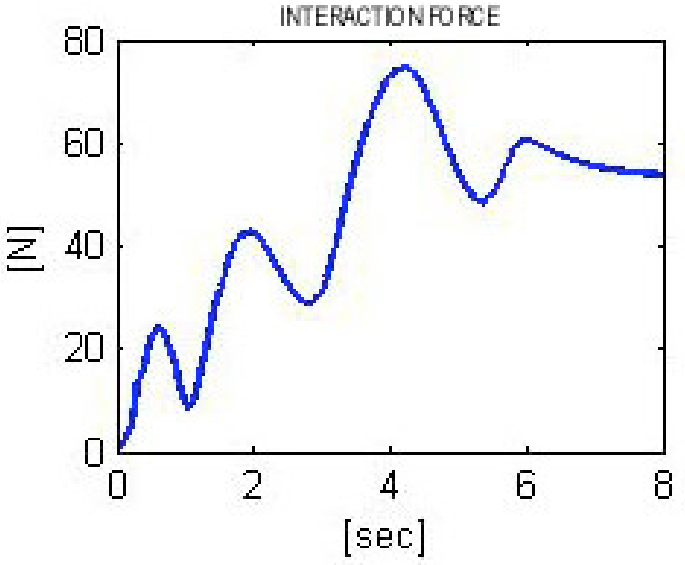

Figure 4.17: Interaction force between the robot arm and the patient in case of severe disability and high control parameters ($F_{dx} = 45$ N, $K_y = 1000$ N/m).

interacting with the robot. The results showed that also in presence of severe disability the control system is capable of counterbalancing incorrect movements, with an efficacy dependent on the control parameters. Future work will be addressed to further investigate performance of the coactivation-based and torque-dependent compliance control by implementing the two control laws on a real operational robotic machine for motor therapy (e.g. the MIT-Manus system) and carrying out clinical trials. Also, the formulation of the control law in the joint space ensures an easy portability of the control law to exoskeletal systems. Thus, an extension and application of the two compliance control to these machines is envisaged.

Domenico Formica

CONCLUSIONS

The application of novel technologies to neurorehabilitaion is expirencing a real breakthrough in the therapy of brain injuries and the interest in this field is continuously growing.

The introduction of properly designed technological solutions and methods could help improving functional recovery in two directions:

- enhancing rehabilitation measurements by quantifying specific pathophysiological mechanisms, spontaneous recovery, functional ability, and therapy dosage more accurately than is now possible;

- giving therapy itself, replicating key components of current manual therapeutic techniques, or even applying new techniques for customizing the therapy on the basis of residual motor capabilities of each single subject.

This dissertation thesis presented innovative methods aimed at supporting the improvement of the current methodologies in both these fields.

From the functional assessment point of view, two different solutions are presented to evaluate patients' level of disability through quantitative, reliable, reproducible mehods.

The VICON stereophotogrammetric system has been used to evaluation of motor impairment of hemiplegic children during pointing tasks. Four subjects were involved in this study, experiments were performed at two different movement speeds with both healthy and plegic arms. A quantitative comparison of motor performance between healthy and plegic patient's arm have been carried out using several evaluation indexes.

Results showed that Movement Duration and Peak Velocity don't highlight any significant difference at low speed, but healthy arms can move faster when fast movements are required. Moreover global characteristics of velocity profiles such as shape (PMR index) and timing (TPV index) are not able to account

Domenico Formica

for differences between healthy and plegic limb; for this reason, they can not be used in this context as evaluation indexes.

On the other hand, the use of the Jerk Index (JI), purposely thought to quantify movement smoothness can strongly discriminate between healthy and plegic behavior in slow movements. Moreover It seems that JI is strongly affected by movement speed so in fast movements JI values of healthy arm assumes higher values with respect to the plegic arm, due to the difference of about 15% in average velocity.

This lack of resolution of JI can be overvome by using the Jerk Cost Function. Values of JCF show a different statistically significant in downward fast movements, where plegic arm exhibits higher values of JCF index. Similar results have been found using the Torque-change Cost Function, that underlines difference between plegic and healthy behavior in slow movements (both upward and downward) as well as in the downward part of the fast movements. This common difference of cost indexes in downward fast movements demonstrate that the brain is not able to optimize Jerk Cost Function and Torque-change Cost Functinon in the same way when controls healthy or plegic limb.

The main goal of the second work was to find a reproducible, quantitative method to estimate the passive stiffness of the wrist joint in healthy subjects and pave the way for further studies with subjects with neuromuscular disorders. The results showed that differences between stiffness in flexed and extended position, as well as abducted and adducted were highly significant in unimpaired subjects, while the PS stiffness appears to be quite symmetrical and the stiffness values are much lower than the two other DOFs.

The two-dimensional stiffness of the combined FE/AA movements has been represented using the stiffness ellipses, which capture the main geometrical features of the elastic force field through three parameters: magnitude (the area), shape (the ratio of the axis) and orientation (direction of the major axis). The magnitude of the ellipses, that represents overall strength of the elastic field, is the only parameter showing a rather high intra- and inter-subject variability. Shape and orientation of the stiffness field seem to be quite invariant across different subjects with anisotropy of 0.7 (ratio between minor and major axis) and confirm the results of the 1-D protocol.

The most novel result relates to the evaluation of the conservative and non-conservative components of the stiffness. The curls of the stiffness matrix, that quantifies the amount of non-conservative energy dissipated to move the wrist along a closed path, were found to be close to zero. The conservative part of the stiffness matrix was found to account for over 99 % of the overall

Domenico Formica

matrix. These results show that the neuromuscular system of the wrist joint is predominantly spring-like; this characteristic of the neuromuscular system has been demonstrated earlier for the other human joints of the upper limb, but to our knowledge, it has never been demonstrated for the wrist joint.

From the motor therapy point of view, a new control approach is proposed to manage interaction in robot-mediated motor therapy of the upper limb, that is purposively conceived for this application field. The control law has been named *torque-dependent compliance control in the joint space* and its applicability to robot-aided motor therapy has been validated in simulation tests as well as in experimental tests.

A first set of tests is used to validate the control law with standard techniques; a comparison with the *coactivation-based compliance control*, used as a reference benchmark to evaluate the performance of the proposed scheme, shows the improvement of the torque-dependent control in situations of contact/ non-contact transition. Trials of robot positioning in the free space and in the constrained space have revealed similar performance of the control laws as regards position regulation. However, for force regulation in presence of unexpected constraints the coactivation-based control appears to be less safe than the torque-dependent compliance control, due to the numerous and sharp spikes in the contact/non-contact transitions.

An application of the torque-dependent compliance control in the joint space to rehabilitation motor therapy has been simulated. The simulator in fact can be also used to simulate different levels of disability of the patient interacting with the robot. The results showed that also in presence of severe disability the control system is capable of counterbalancing incorrect movements, with an efficacy dependent on the control parameters.

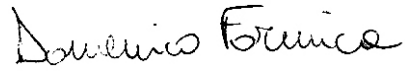

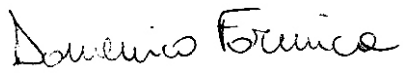

List of Publications

Published

D. Formica, L. Zollo, E. Guglielmelli, "Torque-dependent compliance control in the joint space of a Cartesian robotic machine for motor therapy", *9th IEEE International Conference on Rehabilitation Robotics*, Chicago, Illinois, pp. 341–344, 2005.

D. Formica, L. Zollo, E. Guglielmelli, "Adaptive compliance for enhancing dependability of rehabilitation robotic machines", *4th IARP/IEEE-RAS/EURON Workshop on Technical Challenges for Dependable Robots in Human Environments*, Nagoya, Japan, 2005.

D. Formica, L. Zollo, E. Guglielmelli, "Torque-dependent compliance control in the joint space for robot-mediated motor therapy", *Journal of Dynamic Systems, Measurement, and Control, Transactions of ASME*, vol. 128, pp. 152–158, 2006.

L. Zollo, D. Formica, E. Guglielmelli, "Bio-inspired interaction control of robotic machines for motor therapy", in *Rehabilitation Robotics*, Advanced Robotic Systems Eds., 2007, pp. 619–638.

L. Zollo, D. Accoto, D. Formica, E. Guglielmelli, "Biomechatronic design of dependable systems for rehabilitation robotics", *5th IARP/IEEE-RAS/EURON Workshop on Technical Challenges for Dependable Robots in Human Environments*, Rome, Italy, 2007.

Domenico Formica

Accepted

L. Zollo, D. Accoto, F. Torchiani, D. Formica, E. Guglielmelli, "Design of a Planar Robotic Machine for Neuro-rehabilitation", *2008 IEEE International Conference on Robotics and Automation*, Pasadena, California, 2008.

Submitted

D. Formica, H. I. Krebs, S. K. Charles, L. Zollo, E. Guglielmelli, N. Hogan, "Passive Wrist Joint Stiffness Estimation", Submitted to *The Journal of Neuroscience*, 2008.

Domenico Formica

Bibliography

[1] Heart disease and stroke statistics–2007 update american heart association, dallas, 2007.

[2] Reinkensmeyer DJ, Hogan N, Krebs HI, Lehman SL, Lum PS. *Rehabilitators, Robots, and Guides: New Tools for Neurological Rehabilitation*, chapter in: Biomechanics and Neural Control of Movement, pages 516–533. Springer-Verlag, 2000.

[3] Hasbani MJ, Underhill SM, de Erausquin G, Goldberg MP. Synapse loss and regeneration: a mechanism for functional decline and recovery after cerebral ischemia? *The Neuroscientist*, 6(2):110–119, 2000.

[4] Teasell R, Bayona NA, Bitensky J. Plasticity and reorganization of the brain post stroke. *Topics in Stroke Rehabilitation*, 12(3):11–26, 2005.

[5] Dancause N, Barbay S, Frost SB, Plautz EJ, Chen D, Zoubina EV, Stowe AM, Nudo RJ. Extensive cortical rewiring after brain injury. *The Journal of Neuroscience*, 25(44):10167–10179, 2005.

[6] Brosseau L, Raman S, Fourn L, Coutu-Walkulczyk G, Tremblay L, Beaudoin P. Recovery time of independent poststroke abilities: Part 1. *Topics in Stroke Rehabilitation*, 8(1):60–71, 2001.

[7] Partridge CJ, Johnston M, Edwards S. Recovery from physical disability after stroke: normal patterns as a basis for evaluation. *The Lancet*, 1(8529):373–375, 1987.

[8] Jørgensen HS, Nakayama H, Raaschou HO, Pedersen PM, Houth J, Olsen TM. Functional and neurological outcome of stroke and the relation to stroke severity and type, stroke unit treatment, body temperature, age, and other risk functional and neurological outcome of stroke and

Domenico Formica

the relation to stroke severity and type, stroke unit treatment, body temperature, age, and other risk factors: The copenhagen stroke study.

[9] Nudo RJ. Adaptive plasticity in motor cortex: implications for rehabilitation after brain injury. *Journal of Rehabilitation Medicine*, 41(Suppl):7–10, 2003.

[10] Moskowitz MA, Lo EH. Neurogenesis and apoptotic cell death. *Stroke*, 34(2):324–326, 2003.

[11] Green JB. Brain reorganization after stroke. *Topics in Stroke Rehabilitation*, 10(3):1–20, 2003.

[12] Nudo RJ. Functional and structural plasticity in motor cortex: implications for stroke recovery. *Phys Med Rehabil Clin N Am*, 14(1 Suppl):S57–76, 2003.

[13] Teasell R, Bitensky J, Foley N, Bayona NA. Training and stimulation in post stroke recovery brain reorganization. *Topics in Stroke Rehabilitation*, 12(3):37–45, 2005.

[14] Hallett M. Plasticity of the human motor cortex and recovery from stroke. *Brain Res Rev*, 36(2–3):169–174, 2001.

[15] Carr J, Shepherd R. *A motor relearning programme for A motor relearning programme for stroke*. Oxford: Butterworth Heinemann, 1987.

[16] Schaechter JD. Motor rehabilitation and brain plasticity after hemiparetic stroke. *Prog Neurobiol*, 73(1):61–72, 2004.

[17] Bobath B. *Adult Hemiplegia: Evaluation and treatment*. Heinnemann, London, 1978.

[18] Davies PM. *Steps To Follow*. Springer-Verlag, Berlin, Heidelberg, 1985.

[19] Davies PM. *Right in the Middle, Selective trunk activity in the treatment of adult hemiplegia*. Springer-Verlag, Berlin, 1990.

[20] Brunnstrom S. *Movement Therapy in Hemiplegia: A neurophysiological approach*. Harper and Row, Hargerstown, 1970.

[21] Knott M, Voss DE. *Proprioceptive Neuromuscular Facilitation*. Harper and Row, New York, 1968.

Domenico Formica

[22] Rood M. Neurophysiological reactions as a basis for physical therapy. *Physical Therapy Review*, 34:444–449, 1954.

[23] Johnstone M. *Home Care for the Stroke Patient*. Churchill Livingstone, Edinburgh, 1980.

[24] Wagenaar RC, Meyer OG, Van Wieringen PCW, Kuik DJ, Hazenberg GJ, Lindeboom J, Wichers F, Rijswijk H. The functional recovery of stroke: A comparison between neurodevelopment treatment and the brunnstrom method. *Scandinavian Journal of Rehabilitation Medicine*, 22:1–8, 1990.

[25] Reding MJ, McDowell FH. Focused stroke rehabilitation programmes improve focused stroke rehabilitation programmes improve outcome. *Archives of Neurology*, 46(700–701), 1989.

[26] Twitchell TE. The restoration of motor the restoration of motor function following hemiplegia in man. *Brain*, 74:443–480, 1951.

[27] Nilsson LM, Nordholm LA. Physical therapy in stroke rehabilitation: Bases for swedish physiotherapists, choice of treatment. *Physiotherapy Theory and Practice*, 8:49–55, 1992.

[28] Ernst. A review of stroke rehabilitation and physiotherapy. *Stroke*, 21:1081–1085, 1990.

[29] Wagenaar RC, Meijer OG. Effects of stroke rehabilitation. *Journal of Rehabilitation Science*, 4:61–73, 1991.

[30] Wagenaar RC, Meijer OG. Effects of stroke rehabilitation (2). *Journal of Rehabilitation Science*, 4:97–109, 1991.

[31] Flash T, Hogan N. The coordination of arm movements: an experimentally confirmed mathematical model. *The Journal of Neuroscience*, 5(7):1688–1703, 1985.

[32] Mussa-Ivaldi FA, Hogan N, Bizzi E. Neural, mechanical, and geometric factors subserving arm posture in humans. *The Journal of Neuroscience*, 5(10):2732–2743, 1985.

[33] Uno Y, Kawato M, Suzuki R. Formation and control of optimal trajectory in human multijoint arm movement. minimum torque-change model. *Biological Cybernetics*, 61(2):89–101, 1989.

Domenico Formica

[34] Dario P, Guglielmelli E, Carrozza M C, Micera S, Dipietro L, Pisano F. *Sistemi Sistemi robotici e meccatronici per la neuroriabilitazione*, chapter in: Bioingegneria della postura e del movimento. Patron Editore, Bologna, 2003.

[35] Prange GB, Jannink MJA, Groothuis-Oudshoorn CGM, Hermens HJ, IJzerman MJ. Systematic review of the effect of robot-aided therapy on recovery of the systematic review of the effect of robot-aided therapy on recovery of the hemiparetic arm after stroke. *Journal of Rehabilitation Research and Development*, 43(2):171–184, 2006.

[36] Aisen ML, Krebs HI, Hogan N, McDowell F, Volpe BT. The effect of robot-assisted therapy and rehabilitative training on motor recovery following stroke. *Arch Neurol*, 54(4):443–446, 1997.

[37] Krebs HI, Hogan N, Aisen ML, Volpe BT. Robot-aided neurorehabilitation. *IEEE Transactions on Rehabilitation Engineering*, 6:75–87, 1998.

[38] Volpe BT, Krebs HI, Hogan N, Edelstein OTR L, Diels C, Aisen M. A novel approach to stroke rehabilitation: robot-aided sensorimotor stimulation. *Neurology*, 54(10):1938–1944, 2000.

[39] Fasoli SE, Krebs HI, Stein J, Frontera WR, Hogan N. Effect of robotic therapy on motor impairment and recovery in chronic stroke. *Arch Phys Med Rehabil*, 84:477–482, 2003.

[40] Ferraro M, Palazzolo JJ, Krol J, Krebs HI, Hogan N, Volpe BT. Robot-aided sensorimotor arm training improves outcome in patients with chronic stroke. *Neurology*, 61(11):1604–1607, 2003.

[41] Hogan N, Krebs HI, Rohrer B, Palazzolo JJ, Dipietro L, Fasoli SE, Stein J, Hughes R, Frontera WR, Lynch D, Volpe BT. Motions or muscles? some behavioral factors underlying robotic assistance of motor recovery. *Journal of Rehabilitation Research and Development*, 43(5):605–618, 2006.

[42] Burgar CG , Lum PS, Shor PC, Machiel Van der Loos HF. Development of robots for rehabilitation therapy: The palo development of robots for rehabilitation therapy: The palo alto va/stanford experience. *Journal of Rehabilitation Research and Development*, 37(6):663–673, 2000.

Domenico Formica

[43] Lum PS, Reinkensmeyer DJ, Mahoney R, Rymer WZ, Burgar CG. Robotic devices for movement therapy after stroke: current status and challenges to clinical acceptance. *Topics in Stroke Rehabilitation*, 8(4):40–53, 2002.

[44] Lum PS, Burgar CG, Van der Loos M, Shor PC, Majmundar M, Yap R. Mime robotic device for upper-limb neurorehabilitation in subacute mime robotic device for upper-limb neurorehabilitation in subacute stroke subjects: A follow-up study. *Journal of Rehabilitation Research and Development*, 43(5):631–642, 2006.

[45] Reinkensmeyer DJ, Kahn LE, Averbuch M, McKenna-Cole A, Schmit BD, Rymer WZ. Understanding and treating arm movement impairment after chronic brain injury: Progress with the arm guide. *Journal of Rehabilitation Research and Development*, 37(6):653–662, 2000.

[46] Kahn LE, Zygman ML, Rymer WZ, Reinkensmeyer DJ. Robot-assisted reaching exercise promotes arm movement recovery in chronic hemiparetic stroke: a randomized controlled pilot study. *J Neuroeng Rehabil*, 3:12, 2006.

[47] Hesse S, Sarkodie-Gyan T, Uhlenbrock D. Development of an advanced mechanised gait trainer, controlling movement of the centre of mass, for restoring gait in non-ambulant subjects. *Biomed Tech (Berl)*, 44(7–8):194–201, 1999.

[48] Hesse S, Werner C, Uhlenbrock D, Von Frankenberg S, Bardeleben A, Brandl-Hesse B. An electromechanical gait trainer for restoration of gait in hemiparetic stroke patients: Preliminary results. *Neurorehabil Neural Repair*, 15(1):39–50, 2001.

[49] Pohl M, Werner C, Holzgraefe M, Kroczek G, Mehrholz J, Wingendorf I, Hoölig G, Koch R, Hesse S. Repetitive locomotor training and physiotherapy improve walking and basic activities of daily living after stroke: a single-blind, randomized multicentre trial (deutsche gangtrainerstudie, degas). *Clinical Rehabilitation*, 21(1):17–27, 2007.

[50] Colombo G, Joerg M, Schreier R, Dietz V. Treadmill training treadmill training of paraplegic patients using a robotic orthosis. *Journal of Rehabilitation Research and Development*, 37(6):693–700, 2000.

Domenico Formica

[51] Jezernik S, Schärer R, Colombo G, Morari M. Adaptive robotic rehabilitation of locomotion: a clinical study in spinally injured individuals. *Spinal Cord*, 41(12):657–566, 2003.

[52] Nash MS, Jacobs PL, Johnson BM, Field-Foté E. Metabolic and cardiac responses to robotic-assisted locomotion in motor-complete tetraplegia: a case report. *J Spinal Cord Med*, 27(1):78–82, 2004.

[53] Wirz M, Zemon DH, Rupp R, Scheel A, Colombo G, Dietz V, Hornby TG. Effectiveness of automated locomotor training in patients with chronic incomplete spinal cord injury: a multicenter trial. *Arch Phys Med Rehabil*, 86(4):672–680, 2005.

[54] Colombo G Riener R, Lünenburger L. Human-centered robotics applied to gait training and assessment. *Journal of Rehabilitation Research and Development*, 43(5):679–694, 2006.

[55] Hesse S, Schmidt H, Werner C. Machines to support motor rehabilitation after stroke: 10 years of experience in berlin. *Journal of Rehabilitation Research and Development*, 43(5):671–678, 2006.

[56] Micera S, Carrozza M, Guglielmelli E, Cappiello G, Zaccone F, Freschi C, Colombo R, Mazzone A, Delconte C, Pisano F, Minuco G, Dario P. A simple robotic system for neurorehabilitation. *Advanced Robotics*, 19:271–284, 2005.

[57] Morasso P Solaro C Casadio M, Sanguineti V. A robotic approach for assessing motor adaptation a robotic approach for assessing motor adaptation capability in mild multiple sclerosis patients. In *The first IEEE / RAS-EMBS International Conference The first IEEE / RAS-EMBS International Conference on Biomedical Robotics and Biomechatronics (BIOROB)*, pages 513–518, 2006.

[58] Nef T, Mihelj M, Riener R. Armin: a robot for patient-cooperative arm therapy. *Med Biol Eng Comput*, 45(9):887–900, 2007.

[59] Hingtgen B, McGuire JR, Wang M, Harris JF. An upper extremity kinematic model for evaluation of an upper extremity kinematic model for evaluation of hemiparetic stroke. *Journal of Biomechanics*, 39(681–688), 2006.

Domenico Formica

[60] Hogfors C, Peterson B, Sigholm G, Herberts P. Biomechanical model of the human shoulder joint—ii. the shoulder rhythm. *Journal of Biomechanics*, 24:699–709, 1991.

[61] Schmidt R, Disselhorst-Klug C, Silny J, Rau G. A marker-based measurement procedure for unconstrained wrist and elbow motions. *Journal of Biomechanics*, 32:615–621, 1999.

[62] Andrews JG, Youm Y. A biomechanical investigation of wrist kinematics. *Journal of Biomechanics*, 12:83–93, 1979.

[63] Peterson B, Palmerud G. Measurement of upper extremity orientation by video stereometry system. *Medical and Biological Engineering and Computing*, 34:149–154, 1996.

[64] Biryukova EV, Roby-Brami A, Frolov AA, Mokhtari M. Kinematics of human arm reconstructed from spatial tracking system recordings. *Journal of Biomechanics*, 33:985–995, 2000.

[65] Michaelsen SM, Luta A, Roby-Brami A, Levin MF. Effect of trunk restraint on the recovery of reaching movements in hemiparetic patients. *Stroke*, 32:1875–1883, 2001.

[66] Kamper DG, McKenna-Cole AN, Kahn LE, Reinkensmeyer DJ. Alterations in reaching after stroke and their relation to movement direction and impairment severity. *Arch Phys Med Rehabil*, 83:702–707, 2002.

[67] Adamovich SV, Archambault PS, Ghafouri M, Levin MF, Poizner H, Feldman AG. Hand trajectory invariance in reaching movements involving the trunk. *Experimental Brain Research*, 138:288–303, 2001.

[68] Yang N, Zhang M, Huang C, Jin D. Synergic analysis of upper limb target-reaching movements. *Journal of Biomechanics*, 35:739–746, 2002.

[69] Fritz M. An improved biomechanical model for simulating the strain of the hand-arm system under vibration stress. *Journal of Biomechanics*, 24(12):1165–1171, 1991.

[70] Raikova R. A general approach for modelling and mathematical investigation of the human upper limb. *Journal of Biomechanics*, 25(8):857–867, 1992.

Domenico Formica

[71] Seireg A, Arvikar RJ. A mathematical model for evaluation of forces in lower extremities of the musculo-skeletal system. *Journal of Biomechanics*, 6(3):313–326, 1973.

[72] Zajac FE, Gordon ME. Determining muscle's force and action in multi-articular movement. *Exerc Sport Sci Rev*, 17:187–230, 1989.

[73] Riener R, Straube A. Inverse dynamics as a tool for motion analysis: Arm tracking movements in cerebellar patients. *J Neurosci Methods*, 72(1):87–96, 1997.

[74] Tognetti A, Lorussi F, Bartalesi R, Quaglini S, Tesconi M, Zupone G, De Rossi D. Wearable kinesthetic system for capturing and classifying upper limb gesture in post-stroke rehabilitation. *J Neuroengineering Rehabil*, 2(1):8, 2005.

[75] Murray IA, Johnson GR. A study of the external forces and moments at the shoulder and elbow while performing every day tasks. *Clin Biomech (Bristol, Avon)*, 19(6):586–594, 2005.

[76] Romilly DP, Anglin C, Gosine RG, Hershler C, Raschke SU. A functional task analysis and motion simulation for the development of a powered upper-limb orthosis. *IEEE Trans Rehabil Eng*, 2(3):119–129, 1994.

[77] Winter DA. *Biomechanics and motor control of human movement*. John Wiley & Sons, New York (NY), 1990.

[78] Van der Helm FC. Analysis of the kinematic and dynamic behavior of the shoulder mechanism. *Journal of Biomechanics*, 27(5):527–550, 1994.

[79] Karlsson D, Peterson B. Towards a model for force predictions in the human shoulder. *Journal of Biomechanics*, 25(2):189–199, 1992.

[80] Nieminen H, Niemi J, Takala EP, Viikari-Juntura E. Loadsharing patterns in the shoulder during isometric flexion tasks. *Journal of Biomechanics*, 28(5):555–566, 1995.

[81] Khalili D, Zomlefer M. An intelligent robotic system for rehabilitation of joints and estimation of body segment parameters. *IEEE Trans Biomed Eng*, 35(2):138–146, 1988.

Domenico Formica

[82] Abdullah HA, Tarry C, Datta R, Mittal GS, Abderrahim M. Dynamic biomechanical model for assessing and monitoring robot-assisted upper-limb therapy. *Journal of Rehabilitation Research and Development*, 44(1):43–62, 2007.

[83] Morasso P. Spatial control of arm movements. *Experimental Brain Research*, 42:223–227, 1981.

[84] Bryson AE, Ho YC. *Applied optimal control*. Wiley, New York, 1975.

[85] Nelson WL. Physical principles for economies of skilled movements. *Biological Cybernetics*, 46:135–147, 1983.

[86] Hasan Z. Optimized movement trajectories and joint stiffness in unperturbed, inertially loaded movements. *Biological Cybernetics*, 53:373–382, 1986.

[87] Hogan N. An organizing principle for a class of voluntary movements. *The Journal of Neuroscience*, 4:2743–2754, 1984.

[88] Papaxanthis C, Pozzo T, McIntyre J. Kinematic and dynamic processes for the control of pointing movements in humans revealed by short-term exposure to microgravity. *Neuroscience*, 135(2):371–383, 2005.

[89] Hand trajectories of vertical arm movements in one G and zero-G environments: Evidence for a central representation of gravitational force. Papaxanthis C, Pozzo T, Popov K, McIntyre J. *Experimental Brain Research*, 120:496–502, 1998.

[90] Papaxanthis C, Pozzo T, Schieppati M. Trajectories of arm pointing movements on the sagittal plane vary with both direction and speed. *Experimental Brain Research*, 148:498–503, 2003.

[91] Rohrer B, Fasoli S, Krebs HI, Hughes R, Volpe B, Frontera WR, Stein J, Hogan N. Movement smoothness changes during stroke recovery. *The Journal of Neuroscience*, 22(18):8297–8304, 2002.

[92] Ashworth B. Preliminary trial of carisoprodal in multiple sclerosis. *Practitioner*, 192:540–542, 1964.

[93] Tardieu G, Shentoub S, Delarue R. A la recherché d'une technique de mesure de la spasticité. *Rev Neurol*, 91:143–144, 1954.

Domenico Formica

[94] Wartenberg R. Pendulousness of the legs as a diagnostic test. *Neurology*, 1:8–24, 1951.

[95] Pandyan AD, Johnson GR, Price CI, Curless RH, Barnes MP, Rodgers H. A review of the properties and limitations of the ashworth and modified ashworth scales as measures of spasticity. *Clinical Rehabilitation*, 13:373–383, 1999.

[96] Yam WK, Leung MS. Interrater reliability of modified ashworth scale and modified tardieu scale in children with spastic cerebral palsy. *J Child Neurol*, 21:1031–1035, 2006.

[97] Haugh AB, Pandyan AD, Johnson GR. A systematic review of the tardieu scale for the measurement of spasticity. *Disabil Rehabil*, 28:899–907, 2006.

[98] Krebs HI, Volpe BT, Williams D, Celestino J, Charles SK, Lynch D, Hogan N. Robot-aided neurorehabilitation: A robot for wrist rehabilitation. *IEEE Trans Neural Syst Rehabil Eng*, 15:327–335, 2007.

[99] Hogan N. The mechanics of multi-joint posture and movement control. *Biological Cybernetics*, 52:315–331, 1985.

[100] Dolan JM, Friedman MB, Nagurka ML. Dynamic and loaded impedance components in the maintenance of human arm posture. *IEEE Trans Syst Man Cybern*, 23:698–709, 1993.

[101] Gomi H, Kawato M. Equilibrium-point control hypothesis examined by measured arm stiffness during multijoint movement. *Science*, 272:117–120, 1996.

[102] Gomi H, Osu R. Task-dependent viscoelasticity of human multijoint arm and its spatial characteristics for interaction with environments. jneurosci 18: 8965-8978. *The Journal of Neuroscience*, 18:8965–8978, 1998.

[103] Perreault EJ, Kirsch RF, Acosta AM. Multiple-input, multiple-output system identification for characterization of limb stiffness dynamics. *Biological Cybernetics*, 80:327–337, 1999.

[104] Burdet E, Osu R, Franklin DW, Milner TE, Kawato M. The central nervous system stabilizes unstable dynamics by learning optimal impedance. nature 414: 446 4492001) the central nervous system stabilizes unstable dynamics by learning optimal impedance. nature 414: 446 449 (2001) the

Domenico Formica

central nervous system stabilizes unstable dynamics by learning optimal impedance. *Nature*, 414:446–449, 2001.

[105] De Serres SJ, Milner TE. Wrist muscle activation patterns and stiffness associated with stable and unstable mechanical loads. *Experimental Brain Research*, 86:451–458, 1991.

[106] Sinkjaer T, Hayashi R. Regulation of the wrist stiffness by the stretch reflex. *Journal of Biomechanics*, 22:1133–1140, 1989.

[107] Lakie M, Wlash EG, Wright GW. Resonance at the wrist demonstrated by the use of a torque motor: an instrumental analysis of muscle tone in man. *J Physiol*, 353:265–285, 1984.

[108] Leger AB, Milner TE. Passive and active wrist joint stiffness following eccentric exercise. *Eur J Appl Physiol*, 82:472–479, 2000.

[109] Axelson HW, Hagbarth KE. Human motor control consequences of thixotropic changes in muscular short-range stiffness. *J Physiol*, 535:279–288, 2001.

[110] Gonzalez RV, Buchanan TS, Delp SL. How muscle architecture and moment arms affect wrist flexion-extension moments. *Journal of Biomechanics*, 30:705–712, 1997.

[111] Delp SL, Grierson AE, Buchanan TS. Maximum isometric moments generated by wrist muscles in flexion-extension and radial-ulnar deviation. *Journal of Biomechanics*, 29:1371–1375, 1996.

[112] Simons J,Van Brussel H. *Force Control Schemes for Robot Assembly*, chapter in: Robotic Assembly, pages 253–265. Berlin, Germany, 1985.

[113] Salisbury JK. Active stiffness control of a manipulator in cartesian coordinates. In *Proc. IEEE Conf. Dec. Control*, volume 1, pages 95–100, 1980.

[114] Hogan N. Impedance control: An approach to manipulation - part i, part ii, part iii. *J. Dyn. Syst. Meas. Control, Trans. ASME*, 107:1–24, 1985.

[115] Kazerooni H, Houpt PK, Sheridan TB. Robust compliant motion for manipulators, part 1: The fundamental concepts of compliant motion, part 2: Design method. *IEEE J. Rob. Autom.*, 2:83–105, 1986.

Domenico Formica

[116] Shimoga KB, Goldenberg AA. Grasp admittance center: A concept and its implications. In *IEEE International Conference on Robotics and Automation*, pages 293–298, 1991.

[117] Raibert MH, Craig JJ. Hybrid position/force control of manipulators. *J. Dyn. Syst. Meas. Control, Trans. ASME*, 103:126–133, 1981.

[118] Schneider AYu Gorinevsky DM, Formalsky AM. *Force control of robotics systems*. CRC Press, Boca Raton, 1997.

[119] Formica D, Zollo L, Guglielmelli E. Adaptive compliance for enhancing dependability of rehabilitation robotic machines. In *4th IARP/ IEEE-RAS/EURON Workshop on Technical Challenges for Dependable Robots in Human Environments*, 2005.

[120] Krebs HI, Palazzolo JJ, Dipietro L, Ferraro M, Krol J, Rannekleiv K, Volpe BT, Hogan N. Rehabilitation robotics: Performance-based progressive robot-assisted therapy. *Autonomous Robots*, 15:7–20, 2003.

[121] Katayama M, Kawato M. Virtual trajectory and stiffness ellipse during force trajectory control using a parallel-hierarchical neural network model. In *5th international Conference on Advanced Robotics*, pages 1187–1194, 1991.

[122] Katayama M, Kawato M. Virtual trajectory and stiffness ellipse during multijoint arm movement predicted by neural inverse models. *Biological Cybernetics*, 69:353–362, 1993.

[123] Gomi H, Kawato M. Human arm stiffness and equilibrium- point trajectory during multi-joint movement. *Biological Cybernetics*, 76:163–171, 1997.

[124] Osu R, Gomi H. Multijoint muscle regulation mechanism examined by measured human arm stiffness and emg signals. *J Neurophysiol*, 81:1458–1468, 1999.

[125] Siciliano B, Villani L. *Robot Force Control*. Kluwer Academic, Boston, 1999.

[126] Zollo L, Siciliano B, Laschi C, Teti G, Dario P. An experimental study on compliance control for a redundant personal robot arm. *Robotics and Autonomous Systems*, 44:101–129, 2003.

Domenico Formica

[127] Zollo L, Dipietro L, Siciliano B, Guglielmelli E, Dario P. A bio-inspired approach for regulating and measuring visco-elastic properties of a robot arm. *Journal of Robotic Systems*, 22:397–419, 2005.

[128] Katayama M, Inoue S, Kawato M. A strategy of motor learning using adjustable parameters for arm movement. In *International Conference of the IEEE Engineering in Medicine and Biology Society*, volume 20, pages 2370–2373, 1998.

[129] Baldissera F, Hultborn H, Illert M. *Handbook of Physiology, Section 1: The nervous system*, volume 2. American Physiology Society, Bethesda, 1981.

[130] Serres SJ, Milner TE. Wrist muscle activation patterns and stiffness associated with stable and unstable mechanical loads. *Experimental Brain Research*, 86:451–458, 1991.

[131] Formica D, Zollo L, Guglielmelli E. Torque-dependent compliance control in the joint space of a cartesian robotic machine for motor therapy. In *9th IEEE International Conference on Rehabilitation Robotics*, pages 341–344, 2005.

[132] Formica D, Zollo L, Guglielmelli E. Torque-dependent compliance control in the joint space for robot-mediated motor therapy. *J. Dyn. Syst. Meas. Control, Trans. ASME*, 128:152–158.

[133] Krebs HI, Hogan N, Volpe BT, Aisen ML, Edelstein L, Diels C. Overview of clinical trials with mit-manus: A robot-aided neuro-rehabilitation facility. *Technol Health Care*, 7:419–423, 1999.

[134] Krebs HI, Volpe BT, Aisen ML, Hogan N. Increasing productivity and quality of care: Robot-aided neuro-rehabilitation. *Journal of Rehabilitation Research and Development*, 37:639–652, 2000.

[135] Bhushan N, Shadmehr R. Computational nature of human adaptive control during learning of reaching movements in force fields. *Biological Cybernetics*, 81:39–60, 1999.

[136] Miall RC. *Motor Control, Biological and Theoretical.* The Handbook of Brain Theory and Neural Networks, 1998.

Domenico Formica